Distribution Agreement

In presenting this thesis as a partial fulfillment of the requirements for a degree from Emory University, I hereby grant to Emory University and its agents the non-exclusive license to archive, make accessible, and display my thesis in whole or in part in all forms of media, now or hereafter now, including display on the World Wide Web. I understand that I may select some access restrictions as part of the online submission of this thesis. I retain all ownership rights to the copyright of the thesis. I also retain the right to use in future works (such as articles or books) all or part of this thesis.

Jonathan Giuliano April 15, 2018

# The Role of RNF114 and NF-κB in Chronic Traumatic Encephalopathy (CTE): Experimental Alteration of the Inflammatory Cascade in Cell Culture and Evaluation of a Novel Cellular Trauma Model

by

Jonathan Giuliano

Dr. Chad Hales
Adviser

Neuroscience and Behavioral Biology

Dr. Chad Hales
Adviser

Dr. Michael Crutcher
Committee Member

Dr. Astrid Prinz
Committee Member

2018

# The Role of RNF114 and NF-κB in Chronic Traumatic Encephalopathy (CTE): Experimental Alteration of the Inflammatory Cascade in Cell Culture and Evaluation of a Novel Cellular Trauma Model

by

Jonathan Giuliano

Dr. Chad Hales
Adviser

An abstract of
a thesis submitted to the Faculty of Emory College of Arts and Sciences
of Emory University in partial fulfillment
of the requirements of the degree of
Bachelor of Sciences with Honors

Neuroscience and Behavioral Biology

2018

Abstract

The Role of RNF114 and NF-κB in chronic traumatic encephalopathy (CTE): Experimental Alteration of the Inflammatory Cascade in Cell Culture and Evaluation of a Novel Cellular Trauma Model

By Jonathan Giuliano

Background: The pathological features and clinical presentation of chronic traumatic encephalopathy (CTE) have been explored, but the role of regulatory proteins in the development of CTE remains understudied. Additionally, the limitations of current models of repetitive mild traumatic brain injury (rmTBI) and CTE complicate research efforts. In the present study, we provide a review of current rmTBI and CTE literature, examine the role of RING-type zinc-finger protein 114 (RNF114) and nuclear factor κB (NF-κB) in the inflammatory cascade and their possible link to CTE disease pathogenesis, and test a model for the induction of trauma in cell culture.

Methods: Using immunohistochemistry, tissue sections from the frontal cortices of CTE and Alzheimer's disease (AD) patients were stained for RNF114. Expression of RNF114 and NF-κB in HEK 293T and BV2 cell culture was modified through transfection of plasmids and small interfering RNA (siRNA), and changes in expression were measured through western blotting and quantitative real-time PCR (qPCR). Additionally, the effect of RNF114 up-regulation on tau aggregation was determined through transfection of an RNF114 plasmid in a tau biosensor line and fluorescence resonance energy transfer (FRET) analysis. Finally, a model for the mechanical induction of chronic inflammation in BV2 cell culture was tested, and the long-term effect of agitation of cell culture on expression of RNF114 were measured through western blotting.

Results: Expression of RNF114 in CTE post-mortem brain tissue was significantly depressed, validating the reduction of RNF114 expression previously identified through quantitative proteomics. RNF114 and NF-κB overexpression in BV2 cells found that RNF114 serves as negative regulator of NF-κB. siRNA transfection did not yield a significant depression in RNF114 expression, and as such did not provide insight into the effect of RNF114 knockdown on the inflammatory cascade. Additionally, RNF114 overexpression in a tau biosensor line was not sufficient to promote the aggregation of tau. Finally, we demonstrated a significant increase in expression of RNF114 after agitation of cells in a vortex machine at four and eight days after intervention.

Conclusion: These findings suggest that RNF114 and NF-κB may play a role in the regulation of the neuroinflammatory cascade in CTE and contribute to disease pathogenesis. The results of the mechanical trauma experiments provide a foundation for future studies of cellular rmTBI models.

# The Role of RNF114 and NF-κB in Chronic Traumatic Encephalopathy (CTE): Experimental Alteration of the Inflammatory Cascade in Cell Culture and Evaluation of a Novel Cellular Trauma Model

by

Jonathan Giuliano

Dr. Chad Hales
Adviser

A thesis submitted to the Faculty of Emory College of Arts and Sciences
of Emory University in partial fulfillment
of the requirements of the degree of
Bachelor of Sciences with Honors

Neuroscience and Behavioral Biology

2018

Acknowledgements

I would like to thank Dr. Chad Hales for his mentorship over the past three years and his guidance on this project.

Additionally, I would like to thank James Webster for teaching me the experimental methods I have used during my time in the Hales Lab and for his help procuring the materials used in this study.

I would also like to thank the following individuals for their help with this project: Syed Ali Raza, MBBS, for his help with BV2 maintenance, RNA extraction, cDNA synthesis, and qPCR; Hailian Xiao, for her help with qPCR and data analysis; and Taylor Pohl, for transfection of the RNF114 plasmid in a tau biosensor line and subsequent FRET analysis of tau aggregation.

Finally, I would like to thank the families who donated the brains of their loved ones to scientific research, the Boston University CTE Center for access to CTE tissue samples, and the Emory Alzheimer's Disease Research Center for access to AD tissue samples.

Table of Contents

Tables and Figures

## Introduction and Background

### 1. Overview

While the pathological features and clinical presentation of CTE are better understood, the role of regulatory proteins in the development of CTE remains understudied, and the limitations of current models of rmTBI and CTE complicate research efforts. In the present study, we provide a review of current rmTBI and CTE literature, examine two proteins that regulate neuroinflammation, and test a new model for the induction of mechanical trauma in cell culture.

For nearly a century, repetitive mild traumatic brain injury (rmTBI) has been associated with cognitive impairment (Hales et al., 2014; Martínez-Pérez et al., 2017; Willis and Robertson, 2017). In the 1920s, Harrison Stanford Martland, a forensic pathologist, coined the term 'punch-drunk' to describe the neurobehavioral effects of repetitive head trauma (Martland, 1928). As staining techniques improved in the following decades, the neurophysiological correlates of rmTBI came into focus, and the progressive neurodegeneration associated with rmTBI came to be known as chronic traumatic encephalopathy, or CTE (Critchley, 1949). In recent years, CTE has come to prominence due to its association with contact sports such as football, hockey, and soccer, as well as blast injuries sustained in military combat (Mahar et al., 2017; Pullman et al., 2017; Stern et al., 2011). In the United States, three million concussions are reported each year, and the number of sub-concussive traumas sustained in contact sports are estimated to be far greater - the average lineman, for example, sustains nearly 1,400 sub-concussive impacts over the course of a single season (Barkhoudarian et al. 2016; Gaetz, 2017; McKee and Daneshvar, 2015). Given the high prevalence of concussive and sub-concussive traumas, limiting the incidence of rmTBI must remain a key focus of public health initiatives.

Unique among common neurodegenerative diseases, definitive diagnosis of CTE requires post-mortem examination of brain tissue (Pullman et al., 2017). To this end, the pathophysiology of CTE sheds light on the symptomatology that marks the later life of CTE patients. Microscopic pathology of CTE is characterized by aggregation of hyper-phosphorylated tau (p-tau) in the form of immunoreactive astrocytic and neurofibrillary tangles (NFTs) (Stern et al., 2011). Significant accumulation of amyloid-beta (Aβ) and TAR DNA-binding protein 43 (TDP-43) occurs in some cases, but the contribution of these deposits to the pathogenesis of CTE remains unclear (McKee et al., 2009). Concentrated in the depths of sulci in early stage CTE, extensive tau pathology is found throughout the neocortex, diencephalon, brainstem, and spinal cord in later stages of the disease. Gross pathological features of CTE include a significant reduction in brain weight, atrophy of the neocortex and medial temporal lobe, and enlargement of ventricles and the cavum septum pellucidum (McKee et al., 2009; Mez et al., 2015). In early stage CTE, common symptoms include aggression, depression, memory deficits, and executive dysfunction. In later stages of the disease, individuals may exhibit marked changes in personality and behavior, abnormalities in speech and gait, and progressive dementia (McKee et al., 2009; Stern et al., 2011; Willis and Robertson, 2017).

**2. History of CTE**

In the early 20th century, professional boxing emerged as one of the most popular spectator sports in the United States. After accumulating concussive and sub-concussive traumas during their careers, boxers often entered a period of cognitive decline in later life. Osnato and Gilberti (1927) presented evidence of vasculopathy and gliosis in a post-mortem cohort of one hundred injured brains and introduced the term ‘traumatic encephalitis’, establishing a link between traumatic brain injury and the emergence of neuropathology. Martland (1928) published the first neurological case study of a former professional boxer, a 38-year-old male who had competed

during adolescence and early adulthood. In this study, Martland coined the term 'punch-drunk' to characterize the deficits in motor ability and speech articulation exhibited by the patient. Expanding on Martland's original case study, Millspaugh (1937) introduced the term 'dementia puglistica' to describe the progressive neurodegeneration characteristic of a cohort of lifelong boxers. After World War II, new research highlighted the prevalence of rmTBI in combat operations and in other contact sports, and the neuropathological sequelae of rmTBI came to be known as chronic traumatic encephalopathy (Critchley, 1949; Martínez-Pérez, et al., 2017; McKee et al., 2013).

In the late 1950s and early 1960s, a series of case reports and cohort studies detailing the pathological features of CTE were published in the medical literature. Using new histological techniques, researchers observed significant cerebral atrophy, loss of neuronal density, and propagation of neurofibrillary tangles in the brains of individuals with CTE (McKee et al., 2016). Corsellis et al. (1973), a landmark study of fifteen former boxers, described additional pathological features of CTE, such as ventricular enlargement, callosal thinning, and lesioning of the neocortex. In addition, this study found that severity of pathology correlated directly with the duration of exposure to rmTBI. Omalu et al. (2005), a case study of Mike Webster, a retired football player, sparked new interest in field of CTE research. In the later years of his life, Webster exhibited signs of significant cognitive impairment, struggled with emotional regulation, and attempted suicide on multiple occasions (Gaetz et al. 2017; Omalu et al., 2005). Upon post-mortem examination of Webster's brain, Omalu observed NFTs and tau-positive neuritic threads in the neocortex and diffuse amyloid pathology throughout the brain and diagnosed late-stage CTE (Omalu et al., 2005).

Since publication of Omalu's landmark study, researchers have embarked on a number of post-mortem studies, diagnosing CTE in soccer, hockey, and rugby players, as well as in military

veterans with a history of blast injury (Hales et al., 2014; McKee et al., 2016). After studying tau pathology in individuals with a history of rmTBI, McKee et al. (2013) proposed three criteria for the post-mortem diagnosis of CTE: perivascular aggregation of hyper-phosphorylated NFTs, aggregation of NFTs within cortical sulci, and accumulation of NFTs within the outermost cortical layers. Using these criteria, McKee et al. (2017) evaluated a cohort of 202 football players post-mortem, finding evidence of CTE in 177 players (87%) and, strikingly, in 110 of 111 former NFL players (99%). In time, renewed focus on the clinical presentation and neuropathology of CTE may yield new biomarkers for its diagnosis in living patients as well as new therapies for those afflicted by the disease.

## 3. rmTBI

### 3.1. Overview

Often overlooked as a public health issue, rmTBI represents a significant risk factor for the development of neurological conditions, such as epilepsy, stroke, and Parkinson's disease; through the acceleration of neurodegenerative processes, rmTBI plays a key role in the pathogenesis of CTE (Daneshvar et al., 2013; Faden and Loane, 2015; Wilson et al., 2017). While concussive traumas can cause a loss of consciousness, prolonged confusion, and substantial memory loss, sub-concussive impacts are generally asymptomatic (Ojo et al., 2016). Unimpeded by medical intervention, these traumas can accumulate over time (Daneshvar et al., 2015). As such, rmTBI is best understood as a dynamic process of neurodegeneration, as opposed to a static injury that can be diagnosed at a single point in time (Hutchison et al., 2017; Wojnarowicz et al., 2017). The cumulative effects of rmTBI manifest as a constellation of symptoms and pathological features, such as impairments in sensorimotor and cognitive performance, persistent gliosis, diffuse axonal injury, and a loss of white matter density throughout the brain (Briggs et al., 2016).

Severity of TBI is assessed with a number of metrics, but the most commonly used diagnostic tool in clinical settings is the Glasgow Coma Scale (GCS), often paired with an assessment of post-traumatic amnesia (PTA) and loss of consciousness (LOC) (McKee and Daneshvar, 2015). Using the GCS, medical professionals can grade TBI as mild, moderate, or severe, and an estimated 80% of all traumatic brain injuries are classified as mild (Wojnarowicz et al., 2017). According to the US Department of Veteran Affairs and Department of Defense Clinical Practice Guidelines, a diagnosis of mild TBI is appropriate when the following five criteria are met: (1) duration of LOC in less than 30 minutes, (2) alteration of consciousness is less than 24 hours, (3) the period covered by post-traumatic amnesia is less than one day, (4) patients score between 13 and 15 on the GCS, and (5) structural brain imaging appears normal. As many concussive and sub-concussive traumas go unreported, these guidelines are less reliable for the diagnosis of repetitive traumatic brain injury (rmTBI).

### 3.2. Mechanisms of rmTBI

#### 3.2.1. Biophysics

rmTBI can occur in a variety of situations, and the ultimate development of neuropathology depends on both the severity of each injury and the number of traumas sustained. Studies of closed-head injury in primates have shed light on common biophysical features that characterize the traumatic event (Martínez-Pérez et al., 2017). These studies have shown that rapid linear or angular acceleration of the head can cause the brain to deform within the cranial cavity, leading to axonal stretch injuries, microvascular degeneration, and transient breakdown of the blood-brain barrier (Barkhoudarian et al., 2016; Daneshvar et al., 2015). Due to the gyrencephalic structure of the human brain, impact forces reach their peak in sulci, contributing significantly to the development of neuropathology at the depths of these folds (Morganti-Kossmann et al., 2002). In addition, these

studies indicate that while the impact waves primarily affect forebrain structures, they also affect the midbrain, corpus callosum, and fornix, causing loss of consciousness and amnesia. Furthermore, coup-contrecoup injuries can cause severe focal lesions and elevated intracranial pressure (Martínez-Pérez et al., 2017).

### 3.2.2. Axonal Injury

Axons extend a great distance from the neuronal soma and are especially susceptible to the shearing forces characteristic of rmTBI (Morganti-Kossmann et al., 2002). Whereas severe TBI can cause primary axotomy, or complete transection of the axon, rmTBI tends to cause diffuse axonal injury (DAI), or microscopic damage to the axolemma (Martínez-Pérez et al., 2017). Over time, this loss of structural integrity leads to secondary axotomy and the progressive recession of the axon into the soma (Wojnarowicz et al., 2017). DAI also causes disruptions in axonal function; affected axons exhibit irregular vesicular transport, and calcium influx causes destabilization of microtubules (Barkhoudarian et al., 2016). After destabilization, tau protein dissociates from microtubules, kinases mediate hyperphosphorylation of dissociated tau, and p-tau fragments aggregate and spread throughout the cortex (Martínez-Pérez et al., 2017).

### 3.2.3. Neuroinflammation and Microglial Activation

TBI elicits a complex inflammatory response within the brain; minutes after impact, endogenous glial cells, microglia, and astrocytes activate, proliferate, and migrate to the sites of injury (Faden and Loane, 2015; McKee and Daneshvar, 2015; Woodcock and Morganti-Kossmann, 2013). Microglia have two activation states, M1 and M2, and each state serves a distinct function (Stansley et al., 2012; Byrnes et al., 2012). In the M1 state, microglia secrete pro-inflammatory cytokines such as tumor necrosis factor (TNF), interleukins 1 and 6 (IL-1 and 6), and interferon-gamma (IFN-γ), which promote phagocytosis and support the humoral response

(McKee and Daneshvar, 2015; Ziebell and Morganti-Kossmann, 2010). In the M2 state, microglia secrete anti-inflammatory cytokines such as TGF-β, IL-4 and IL-10, which suppress the initial M1 inflammatory response and promote tissue repair within the injured area (Stansley et al., 2012; Wojnarowicz et al., 2017; Woodcock and Morganti-Kossmann, 2013; Zhang et al., 2013). Dohi et al. (2010) found that NOX2, which suppresses the M1/M2 transition, is chronically activated in individuals with a history of rmTBI. Other studies have shown that perivascular microgliosis and astrocytosis persist for months after a traumatic event (Briggs et al., 2016; Byrnes et al., 2012; Morganti-Kossmann et al., 2002). Taken together, these processes promote chronic neuroinflammation, which has been linked to the development of p-tau pathology in CTE (Cherry et al., 2016).

Post-mortem cohort studies suggest that neuroinflammation and microglial activation, while protective in the short term, play a significant role in the long-term development of neuropathology after rmTBI. Using positron emission tomography (PET), Ramalackhansingh et al. (2011) found evidence of increased microglial activation throughout the brain up to seventeen years after TBI in a cohort of living patients; binding of the PK ligand was significantly increased in the thalamus, putamen, and occipital cortex compared to control. Drawing from the Glasgow Traumatic Brain Injury archive, Johnson et al. (2013) observed densely packed clusters of immunoreactive microglia in 28% of cases and a significant reduction in the thickness of the corpus callosum in 25% of cases, with survival of up to eighteen years post-trauma.

Studies of closed-head injury in rodent models have provided additional support for these findings. In one study, Shitaka et al. (2011) monitored areas adjacent to axons after rmTBI, finding that reactive microglia preferentially localized to these areas in the weeks after traumatic brain injury. In a second study, Loane et al. (2014) observed chronically active microglia at the

expanding margins of the injury site one year after traumatic brain injury, accompanied by a significant reduction in hippocampal volume and degeneration of white matter tracts. In a third study, Mouzon et al. (2014) found that markers of chronic neuroinflammation correlated with severe cognitive deficits up to 18 months after initial trauma, and diffusion tensor imaging revealed severe damage to white matter tracts throughout the brain.

As chronic microglial activation plays a key role in the inflammatory cascade after TBI, recent studies have attenuated activation of microglia and measured the effect of these interventions on neurodegenerative processes. Using an mGluR5 agonist to inhibit microglial activation, Byrnes et al. (2012) found a significant reduction in inflammation, neuronal loss, and lesion volume at four months post trauma. In another study, Piao et al. (2013) found that moderate exercise after traumatic brain injury inhibited NOX2 activity, attenuating microglial activation and avoiding subsequent neurodegeneration. Taken as a whole, these studies suggest that anti-inflammatory intervention after rmTBI may limit the emergence of neuropathology.

**3.2.4. Other Contributors to Neuropathology**

Increases in membrane permeability after injury promote excessive intracellular calcium influx and potassium efflux and elicit the release of excitatory neurotransmitters, such as glutamate, throughout the brain (Barkhoudarian et al., 2016; Faden et al., 1989). To normalize membrane potentials, ATP-dependent Na/K pumps become overactive, increasing glucose metabolism (Daneshvar et al., 2015). Post-traumatic hyper-metabolism of glucose entails excessive production of lactate, which leads to cerebral edema and increased intracranial pressure (Faden et al., 1989; Morganti-Kossmann et al., 2002). In addition, damage to blood vessels may affect the network of perivascular channels that make up the glymphatic system. Iliff et al. (2014) found that function of the glymphatic system is reduced up to 60% after TBI, limiting clearance

of tau and promoting development of neurofibrillary pathology. Indeed, researchers found that levels of cortical p-tau were elevated up to 28 days after traumatic brain injury.

## 4. CTE

### 4.1. Diagnosis and Prevalence

Currently, a definitive diagnosis of CTE is only possible upon post-mortem examination of brain tissue (Huber et al., 2016). While preliminary criteria for clinical diagnosis have been proposed - a history of rmTBI, evidence of cognitive or sensorimotor decline, and a positive neurological exam - biomarkers specific to CTE have not been discovered (Gaetz, 2017). In the absence of known biomarkers, diffusion tensor imaging (DTI) is used to assess axonal integrity in patients with a history of rmTBI, and cognitive deficits have been associated with a significant loss of white matter density (McKee et al., 2009).

As human studies of CTE are conducted using donated brain tissue, sampling bias complicates attempts to determine the prevalence of CTE (Gaetz, 2017). Striking results of post-mortem studies, such as the 99% prevalence of CTE recently observed in a sample of former NFL players (McKee et al., 2017), cannot be extrapolated to living cohorts, and attempts to do so will inevitably overestimate the true incidence of CTE. If CTE-specific biomarkers are discovered in the future, researchers will be able to estimate the prevalence of CTE in living populations for the first time.

### 4.2. Stages of CTE

In stage I of CTE, perivascular clusters of p-tau NFTs are found at the depths of sulcal folds in the frontal and temporal cortices (Daneshvar et al., 2015; Huber et al., 2016). Clinically, stage I involves minor cognitive dysfunction and gradual changes in mood and behavior (Mahar et al., 2017). Common symptoms include persistent headache, deficits in attention and memory, and

increased aggression (McKee et al., 2013). By stage II, p-tau NFTs spread to superficial cortical layers adjacent to the initial foci. During this stage, patients display increased aggression that gives way to explosive outbursts, and depression and suicidal ideation become common (Mahar et al., 2017; McKee et al., 2013). In stage III, p-tau NFTs are found throughout the frontal, temporal, and parietal cortices, and structures within the medial temporal lobe, such as the hippocampus, entorhinal cortex, and amygdala, begin to show signs of NFT-mediated neurodegeneration. In addition, NFTs spread to the olfactory bulbs, hypothalamus, thalamus, substantia nigra, and the dorsal and median raphe nuclei (Daneshvar et al., 2015; Huber et al., 2016). Cerebral atrophy and ventricular dilation also occur at this stage (McKee et al., 2013). Clinically, cognitive impairment becomes more severe; individuals display significant deficits in executive function, memory recall, attention, and concentration (Mahar et al., 2017). In Stage IV, dense clusters of NFTs are found throughout the brain, accompanied by a significant reduction of neuronal density in the hippocampus and the demyelination of white matter tracts (Daneshvar et al., 2015; Huber et al., 2016). In addition, severe p-tau pathology is observed throughout the cortex, basal ganglia, brainstem, and spinal cord, and ventricles continue to dilate as the brain atrophies (McKee et al., 2013). Affected individuals display signs of severe dementia, executive dysfunction, and aggression, and they may become severely paranoid, depressed, or suicidal at this stage (Mahar et al., 2017).

### 4.3. Clinical Presentation

#### 4.3.1. Overview

Symptoms of CTE develop slowly over time, emerging years or decades after rmTBI exposure (Mahar et al., 2017; McKee et al., 2009; Stern et al., 2011). Onset of CTE typically occurs earlier than that of Alzheimer's Disease (AD) or frontotemporal dementia (FTD); in one study of

119 confirmed CTE cases, average age at symptom onset was 44 years (Huber et al., 2016). After a long latent period, impairments in cognitive and motor function tend to develop first, complicated by marked changes in mood and behavior as the disease progresses (Martínez-Pérez et al., 2017; Mez et al., 2015). Severity and progression of clinical presentation appears to correlate with both the number of traumas sustained by the patient and the duration of exposure to repetitive trauma (McKee et al., 2009). Co-morbid neurological disorders are common and include AD, Parkinson's disease (PD), motor neuron disease (MND), frontotemporal lobar degeneration (FTLD), and Lewy Body disease (LB) (Faden and Loane, 2015; Ojo, 2016).

**4.3.2. Cognitive and Behavioral Changes**

Cognitive symptoms of CTE typically emerge around middle age, and persistent headache is an early and prominent system in almost half of all individuals with early-stage CTE (Faden and Loane, 2015; Martínez-Pérez, et al., 2017). Progressive degeneration of the frontal and medial temporal lobes causes impairments in executive function and memory recall; degeneration of the amygdala and orbitofrontal cortex can cause marked changes in mood and behavior (McKee et al., 2009). Individuals with executive dysfunction and memory impairment may notice deficits in their ability to plan, organize, multitask, and judge situations appropriately (Stern et al., 2014). In addition, deficits in emotional regulation may lead to social anxiety and reclusive behavior, sudden changes in personality, and frequent episodes of irritability and aggression (Gaetz, 2017).

As CTE progresses, motor deficits become prevalent. Individuals may present with slurred or telegraphic speech (dysarthria), have difficulty swallowing (dysphagia), and exhibit difficulties with coordination (ataxia) (McKee et al., 2009; Stein et al., 2015). As damage to the cerebellum and substantia nigra pars compacta becomes more severe in late-stage CTE, individuals may develop Parkinsonian symptoms, presenting with a persistent tremor, decreased emotional affect,

and muscle rigidity (Huber et al., 2016). In addition, psychiatric symptomatology in CTE can complicate diagnosis and treatment (Mez et al., 2015). Major depression and suicidal ideation are common, with prevalence of up to 33% in some cohorts - nearly ten times that of the general population (Gaetz, 2017).

### 4.4. Neuropathology

#### 4.4.1. Overview

In 2015, the National Institutes of Health convened a meeting to determine the neuropathological criteria for diagnosis of CTE (McKee et al. 2016). During this meeting, seven neuropathologists evaluated a randomized set of 25 tauopathies using the following preliminary criteria proposed by McKee et al. (2013):

*(i) perivascular foci of p-tau immunoreactive astrocytic tangles and neurofibrillary tangles*

*(ii) irregular cortical distribution of p-tau immunoreactive neurofibrillary tangles and astrocytic tangles with a predilection for the depth of cerebral sulci*

*(iii) clusters of subpial and periventricular astrocytic tangles in the cerebral cortex, diencephalon, basal ganglia and brainstem*

*(iv) neurofibrillary tangles in the cerebral cortex located preferentially in the superficial layers*

Building upon these criteria, the working group attempted to distinguish CTE from other common tauopathies, finding that the presence of perivascular p-tau tangles in neurons, astrocytes, and cellular projections concentrated within the sulcal depths constituted a pathognomonic feature of CTE. In addition, the group found evidence of NFT-mediated hippocampal degeneration, diffuse amyloid plaques, and deposits of phosphorylated TDP-43, co-localized with p-tau, throughout the brain. Other supportive features found include the presence of immunoreactive pretangles in the superficial layers of the neocortex (II-III) as well as NFTs within the hippocampus (regions CA2

and CA4), amygdala, nucleus accumbens, thalamus, and midbrain (McKee et al. 2016). Taken as a whole, these neuropathological criteria may lead to greater standardization of diagnosis in post-mortem studies.

**4.4.2. Microscopic Neuropathology**

As discussed above, CTE is characterized by the perivascular deposition of p-tau in the form of neurofibrillary and argyrophilic tangles (ATs), thorned astrocytes (TAs), and neuropil neurites (NTs), most commonly observed in the sulcal depths of the frontal and temporal cortices and in the superficial layers surrounding these foci (Huber et al., 2016). In early-stage CTE, perivascular clusters of activated microglia are observed in the subcortical white matter and become more dense and numerous as the disease progresses (Daneshvar et al., 2015). In late-stage disease, deposits of TDP-43, co-localized with p-tau, are found throughout the brain, and in some cases, deposits of Aß are observed (Huber et al., 2016).

While the contribution of Aß plaques to the development of CTE is unclear, immunoreactive TDP-43 inclusions and neurites in the brainstem, basal ganglia, diencephalon, and medial temporal lobe have been linked to the emergence of co-morbid motor neuron disease (MND) (McKee et al., 2010; Stern et al., 2011). Loss of neuronal density and persistent gliosis have been shown to occur throughout the brain, most notably in the hippocampus (CA1 and subiculum), substantia nigra, cerebral cortex, and amygdala (McKee et al., 2009).

**4.4.2.1. Tau**

Part of a family of microtubule-associated proteins (MAPs), tau protein assists in the assembly and stabilization of axonal microtubules (Nizynski et al., 2017). Kinases and phosphatases play a key role in the regulation of normal tau function and the development of tau pathology (Rubenstein et al., 2017). After traumatic brain injury, intracellular calcium influx and

glutamate receptor-mediated excitotoxicity cause tau to dissociate from microtubules; dissociated tau is subsequently phosphorylated, folded, and cleaved by a variety of endogenous kinases, calpains, and caspases (McKee et al., 2013; Amadoro et al., 2006). After initial processing, these p-tau fragments link together, forming paired helical fragments (PHFs) which aggregate further into neurofibrillary tangles (NFTs) (Nizynski et al., 2017).

In CTE, NFTs, neuropil threads, and astrocytic tangles concentrate in the frontal and temporal lobes, impairing executive function and memory retrieval, and ultimately spread throughout the cerebral cortex, midbrain, and brainstem (Faden and Loane, 2015; Kanaan, et al. 2011; Seo et al., 2017). Recent studies of interneuronal tau transfer suggest that p-tau fragments propagate through templated misfolding, suggesting prion-like transmission of tau pathology (Chen et al., 2010; Manavalan et al., 2013; Wojnarowicz et al., 2017). Other proposed mechanisms include synaptic transmission, paraventricular migration, and glymphatic transport (McKee et al., 2013).

**4.4.2.2. TDP-43**

TDP-43 is a common DNA- and RNA-binding protein involved in the stabilization of mRNA after axonal injury; dysregulation of TDP-43 has been linked to the emergence of tau pathology (Daneshvar et al., 2015; Huber et al., 2016). Studies of axonal injury have shown that traumatic axotomy, characteristic of severe and repetitive TBI, increases expression and accelerates aggregation of TDP-43 within the brain (Huber et al. 2017). Immunoreactive TDP-43 deposits are found in nearly 80% of CTE cases, from sparse deposits in early-stage CTE to intraneuronal and intraglial inclusions throughout the brain in late-stage CTE (McKee et al., 2013).

Deposition of TDP-43 has been linked to the development of motor neuron disease, found in 10-13% of CTE cases (McKee et al., 2010). TDP-43 deposits interfere with the normal function

of the frontal and temporal cortices, medial temporal lobe, basal ganglia, diencephalon, brainstem, and spinal cord, leading to profound muscle weakness, atrophy, and loss of muscle control (McKee and Daneshvar, 2015). As TDP-43 plays a key role in the pathogenesis of CTE-MND, further research is needed to uncover therapies that limit the accumulation and aggregation of TDP-43 after rmTBI.

#### 4.4.2.3. Amyloid-Beta

In CTE, deposition of amyloid-beta (Aβ) is less common than deposition of tau and TDP-43, and the role of Aβ in the pathogenesis of CTE is highly controversial (Ojo, 2016). Once thought to be a universal feature of CTE (McKee et al., 2009), Aβ deposits are now thought to be present in only a subset of cases (Daneshvar et al., 2015; Stein et al., 2015). Huber et al. (2016) observed diffuse or neuritic Aβ plaques in 52% of CTE cases, finding that individuals with CTE were 3.8 times more likely to develop Aβ plaques than those without CTE. In addition, researchers found that Aβ deposition in CTE was associated with presence of the APOE ε4 allele, older age at onset, and older age at death. Controlled for age, the presence of neuritic plaques was associated with severity of CTE as well as the development of Lewy body disease and dementia. Other studies suggest that the severity of rmTBI correlates with the degree of Aβ pathology (Daneshvar et al., 2014; Faden and Loane, 2015). At this time, the link between Aβ pathology and the severity of CTE is unclear; further research is needed to determine whether Aβ deposition is a primary driver or ancillary marker of the pathogenesis of CTE.

### 4.4.3. Gross Neuropathology

Generally, gross abnormalities are only visible in late-stage CTE. The most visible of these abnormalities include a reduction in brain weight (~200 grams), atrophy of the frontal, temporal, and parietal lobes, dilation of the lateral and third ventricles, and thinning of the corpus callosum

(Huber et al., 2016). Other visible features include depigmentation of the substantia nigra and locus ceruleus, scarring of the cerebellum and septum pellucidum, and atrophy of the diencephalon, thalamus, brainstem, and cerebellum. In severe cases, atrophy of the hippocampus, amygdala, and entorhinal cortex is observed (McKee et al., 2009).

**4.5. Risk Factors**

Exposure to rmTBI is the main risk factor for the development of CTE, but it is not the only risk factor; all individuals with CTE have a history of rmTBI, but not everyone with exposure to rmTBI develops CTE (Stern et al., 2011). Recent studies suggest that genetic risk factors may influence the development of CTE. Involved in the transport of lipids and clearance of neural metabolites, apolipoprotein E (APOE) is significantly associated with the pathogenesis of AD and other neurodegenerative diseases (Stern et al., 2013). Recent studies have linked the presence of the APOE ε4 allele to length of recovery and severity of cognitive deficits after TBI (Daneshvar et al., 2015), but the correlation between APOE ε4 and severity of CTE remains to be determined (Martínez-Pérez et al., 2017; Stein et al., 2015).

Duration of exposure to rmTBI, severity of trauma, and age at injury are three prominent behavioral risk factors for CTE (Ojo, 2016). Current research suggests that there is a positive correlation between duration of exposure to rmTBI and severity of ultimate neuropathology (McKee et al., 2009). In addition, exposure to and severity of traumatic impacts can vary based on the type of sport and position played. For example, professional boxers sustain more head trauma than football players on average, and linemen sustain far more impacts in practice and during games than do other players (Stern et al., 2011). Furthermore, age at time of injury has been found to have a profound effect on the ultimate development of CTE. While one may assume that greater functional plasticity at an earlier age would allow for a quicker and more substantial recovery,

current research suggests that younger brains are more susceptible to diffuse injury, which can lead to more severe cognitive deficits (Stein et al., 2015; Stern et al., 2011). Lifestyle choices and preexisting conditions may also play a role in the pathogenesis of CTE. Abuse of alcohol, recreational drugs, and performance-enhancing drugs (PEDs) is linked to the development of cognitive difficulties, and the chronic inflammation characteristic of obesity, diabetes, and heart disease drives neurodegenerative processes and promotes formation of NFTs (Baugh et al., 2014; Huber et al., 2016).

**5. Regulation of the Neuroinflammatory Cascade**

While the neurotoxic effects of chronic inflammation have been well established, the proteins that regulate the neuroinflammatory cascade in CTE have not been well studied. Exploration of the CTE insoluble proteome yields two promising candidates - NF-κB, a transcriptional regulator of the inflammatory cascade, and RNF114, a negative regulator of NF-κB - both highly expressed within microglia (Hales et al., 2017; Zhang, 2014). NF-κB mediates the immune response, promotes cell proliferation, and inhibits apoptosis through up-regulation of survival genes (A1, PAI-2, IAP) and anti-apoptotic proteins (Bcl-xL) (Gilmore et al., 2006; Perkins et al., 2000). Sustained expression of NF-κB leads to chronic inflammation, contributing to a wide range of autoimmune diseases, cancers, and neurological disorders (Perkins et al., 2006).

To limit chronic inflammation within the body, A20, a cytoplasmic protein, regulates NF-κB expression through a negative feedback loop (Vereecke et al., 2009; Shembade et al., 2012; Rodriguez et al., 2014). Expression of NF-κB promotes up-regulation of A20, and A20 subsequently deactivates NF-κB (Renner et al., 2009). Stability of A20 is highly important; down-regulation of A20 has been implicated in the pathogenesis of autoimmune diseases such as Crohn's disease, psoriasis, and lupus (Stuart et al., 2010, Vereecke et al., 2011; Verstrepen et al., 2010).

RNF114, a RING domain ubiquitin ligase, has been shown to stabilize A20 (Rodriguez et al., 2014). When expression of RNF114 is down-regulated in cells, A20 becomes unstable, leading to constitutive expression of NF-κB and prolonged activation of the inflammatory cascade. As RNF114 is expressed within microglia and reduced in the insoluble proteome of CTE across all stages of disease, further study of the relationship between NF-κB and RNF114 could shed light on the role of each in the promotion of chronic neuroinflammation **(Figure 1)**.

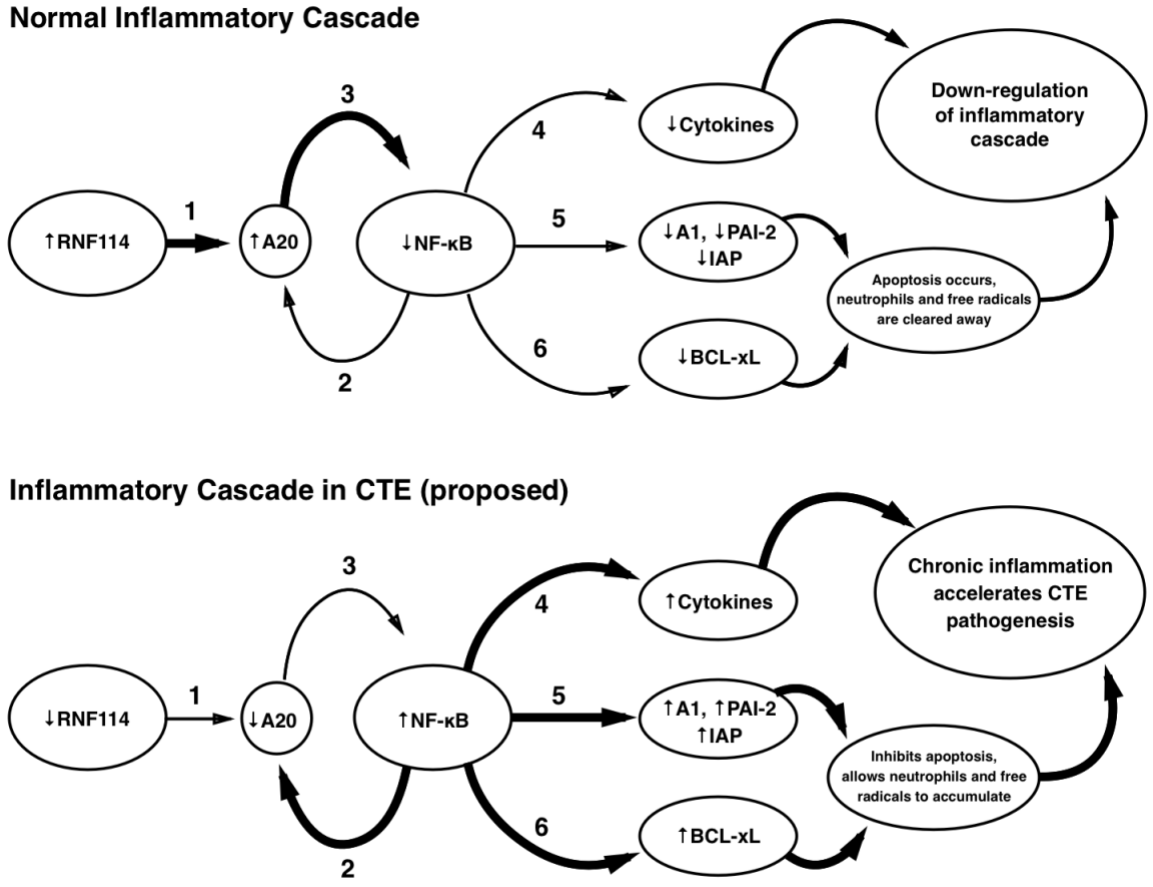


**Figure 1. Role of RNF114 and NF-κB in the neuroinflammatory cascade**

RNF114, a RING domain ubiquitin ligase, promotes up-regulation of A20, a negative regulator of the inflammatory cascade, through ubiquitination of the E3 ligase domain (1). Expression of NF-κB, a primary driver of the inflammatory response, also promotes up-regulation of A20 (2), and A20 subsequently deactivates NF-κB (3). NF-κB mediates immune response through the release of cytokines (4) and inhibits apoptosis through upregulation of survival genes such as A1, PAI-2, and IAP (5) and anti-apoptotic proteins such as Bcl- xL (6). When expression of RNF114 is downregulated after rmTBI, A20 becomes unstable, leading to constitutive expression of NF-κB, prolonged activation of the neuroinflammatory cascade, and acceleration of CTE pathogenesis.

**5.1. NF-κB**

Discovered by Sen and Baltimore (1986), nuclear factor-κB (NF-κB) was first thought to regulate activity of the κ light chain enhancer in B cells; subsequent studies have found that NFκB plays a role in both adaptive and innate immunity (Harhaj and Dixit, 2012). As a central regulator of the inflammatory cascade, nuclear factor-κB (NF-κB) is involved in many cellular processes, including proliferation, apoptosis, angiogenesis, and immune response (Housley et al., 2015). Dysregulation of NF-κB has been implicated in the pathogenesis of multiple cancers (ovarian, lung, gastric, breast, and retinoblastoma) as well as asthma, multiple sclerosis, rheumatoid arthritis, and the influenza A virus (Chen et al., 2015; Dam et al., 2016; Housley et al., 2015; Kanzaki et al., 2016; Li et al., 2015; Perkins et al., 2000; Zaynagetdinov et al, 2016). Conserved across species, the NF-κB family consists of five proteins - p50, p52, p65 (RelA), RelB, and c-Rel - all of which share a DNA binding and dimerization sequence, the Rel homology domain (RHD) (Gilmore, 2006; Perkins et al., 2000). While the p50/p65 heterodimer is the most common active form of NF-κB, homo- and heterodimers of NF-κB proteins are ubiquitously expressed and induced by a wide range of stimuli (Harhaj and Dixit, 2012; Perkins and Gilmore, 2006).

In quiescent cells, NF-κB complexes are sequestered in the cytoplasm by inhibitory IκBα proteins (Harhaj and Dixit, 2012, Vereecke et al., 2009). In the presence of pathogenic stimuli such as lipopolysaccharide (LPS), TNF and IL-1, the IκB kinase (IKK) complex, which consists of two catalytic subunits (IKKα and IKKβ) and a regulatory subunit (IKKγ, or NEMO), is recruited and activated (Perkins and Gilmore, 2006). The activated IKK complex phosphorylates the inhibitory IκBα proteins, and these proteins are subsequently degraded by the cell. After elimination of IκBα, NF-κB complexes translocate to the nucleus of the cell and induce transcription of target genes,

which include TNF and IL-1, promoting the amplification of the NF-κB signal in a positive feedforward loop (Renner and Schmitz, 2009).

**5.2 Regulation of NF-κB**

As NF-κB plays a crucial role in the regulation of many cellular processes, a complex system of feedback loops guides the termination of the NF-κB signaling cascade, preventing chronic inflammation (Vereecke et al., 2009). To this end, a number of positive and negative regulators are released after activation of NF-κB to allow for temporal and spatial regulation of the signaling pathway (Renner and Schmitz, 2009). Of these, three deubiquitinases - A20, Cezanne, and CYLD - are the most prominent regulators of NF-κB expression (Li et al., 2015; Harhaj and Dixit, 2012). A20, also known as TNF-α inducible protein 3 (TNFAIP3), is activated by pro-inflammatory cytokines and inhibits the NF-κB signaling cascade through the removal of polyubiquitin chains (Vereecke et al., 2009, Verstrepen et al., 2010). In a similar fashion, Cezanne and CYLD are activated by pro-inflammatory cytokines in the environment and mediate the removal of ubiquinated side chains (Harhaj and Dixit, 2012). In addition, dysregulation of A20 and other deubiquitinases has been implicated in the pathogenesis of multiple inflammatory diseases, such as Crohn's disease, rheumatoid arthritis, psoriasis, and systemic lupus (Vereecke et al., 2009).

**5.3. RNF114**

RING-type zinc-finger protein 114 (RNF114), part of a family of RING domain E3 ubiquitin ligases, is characterized by three zinc-binding fingers and one ubiquitin-interacting motif (UIM) (Rodriguez et al, 2014). In the cell, RNF114 is a negative regulator of the NF-κB signaling cascade, stabilizing A20 and IκBα though ubiquitylation (Han et al., 2013). To this end, expression of RNF114 is stimulated by pro-inflammatory cytokines, such as IFNα and IFNγ. In addition,

RNF114 has been shown to trigger apoptosis, stimulate the G1/S and G2/M transitions of the cell cycle, and influence the cellular stress response (Bijlmakers et al., 2011).

**6. Models of rmTBI and CTE**

Animal and cellular models are commonly used for the study of rmTBI and CTE. While the generalizability of rodent studies is limited by differences in the physiology of humans and rodents, humans and mice share significant homology in coding genes, and gene structure and order are highly conserved between the species (Wojnarowicz et al., 2017). As such, mice are widely used to study the neurophysiological correlates of acute and repetitive TBI and the regulation of the neuroinflammatory cascade. Interventions used to model acute TBI include fluid percussion injury (FPI), controlled cortical impact (CCI), and the Marmarou weight drop model; these models employ hydraulic pressure, pneumatic pistons, and weights of known mass, respectively, to induce diffuse axonal injury, release of pro-inflammatory cytokines, reactive gliosis, and neurobehavioral changes (Byrnes et al., 2012; Goldstein et al., 2012; Ojo, 2016). Studies of rmTBI have revised the weight drop model to administer repeated cortical impacts within a predetermined time frame (Briggs et al., 2016).

While studies of animal models have shed light on the mechanisms of acute and repetitive TBI, they require regulatory approval, significant time for preparation, and are prohibitively expensive for many labs. As such, cellular models of rmTBI and CTE have become popular in recent years. In the mechanical stretch injury model, researchers seed cells on collagen-coated silastic membranes, then stretch the membranes to study the effects of stretch injury on cell viability and morphology (Xu et al., 148). While this intervention promotes diffuse axonal injury, inflammation, and cellular senescence, it does not account for the primary axonal injury after rotational acceleration of the cranial cavity found in rmTBI. To study microglial response,

researchers have derived a number of microglial cell lines: primary microglia, BV2 and N9 immortalized microglia, human immortalized microglia (HMO6), and spontaneously immortalized rodent microglia (EOC and HAPI) (Stansley et al., 2012). Of these, BV2 cells offer superior stability and doubling time and accurately model microglial response to inflammatory stimuli in vitro (Henn et al., 2009).

**7. Rationale and Hypotheses**

While the pathology and symptomology of CTE have been thoroughly explored in the literature, the regulatory factors that influence the development of CTE remain understudied. Our initial exploration of the CTE brain insoluble proteome found two promising candidates, NF-κB, a driver of the inflammatory cascade, and RNF114, a negative regulator of NF-κB (Hales et al., 2017; Zhang, 2014). In addition, current models of rmTBI and CTE have limitations. Animal models are resource- and time-intensive, while cellular models often fail to accurately capture the linear and angular acceleration characteristic of rmTBI. As a result, the present study will address the possible role of RNF114 and NF-κB in CTE in addition to establishing a novel model of rmTBI. First, we aim to provide a comprehensive review of current rmTBI and CTE literature, focusing on the history of CTE research, the neuropathology of rmTBI, and the pathological features and clinical presentation of CTE. Second, we will test the hypothesis that RNF114 alters NF-κB expression by modifying the expression of RNF114 and NF-κB in HEK 293T and BV2 cells with overexpression and siRNA. Additionally, we will test the hypothesis that RNF114 affects tau aggregation by quantifying the effect of RNF114 up-regulation on tau aggregation (a key feature of CTE pathology) in a YFP/CFP HEK 293T tau biosensor line. Third, we will test the hypothesis that mechanical agitation of BV2 cells will alter long-term expression of RNF114, up-regulate the

inflammatory cascade and provide a cell culture model of rmTBI. Findings from these studies will improve our understanding of cellular mechanisms that contribute to CTE.

## Materials and Methods

### 1. Cell Lines

#### 1.1. BV2

Primary microglia (PM) are commonly used to study microglial activation in vitro. However, isolation of a primary microglial cell line is both time- and resource-intensive. Preparation of PM culture may require up to thirty rodent brains, and researchers must prepare a new PM culture for each set of experiments, as each culture has a limited capacity for proliferation. The significant lead time and expense involved in preparation of PM culture limits the number of PM experiments a research group can conduct in a given time; as such, there is a clear need for immortalized cell culture lines that accurately model primary microglial response in vitro (Henn et al., 2009). To meet this need, Blasi et al. (1990) created the immortalized BV2 cell line, transforming a standard murine microglial cell line using a raf/myc retrovirus. As BV2 cells can model the response of PM to inflammatory stimuli and signaling molecules with high fidelity, they have become the most frequently used substitute for primary microglia in the years since their discovery (Henn et al., 2009). In the present study, BV2 cells were used to study protein expression and the inflammatory cascade.

#### 1.2. HEK 293T and YFP/CFP

Human embryonic kidney (HEK) 293 cells are an immortalized human cell line, known for robust growth and high transfection efficiency (Shaw et al., 2002). To create this line, Graham et al. (1973) transformed cultures of primary HEK cells using fragments of adenovirus 5 (Ad5) DNA. Commonly used in studies of protein expression, HEK 293 cells work well with a variety

of transfection protocols (lipid, calcium phosphate, electroporation) and gene vectors (plasmids, adenoviruses, siRNA) (Shaw et al., 2002). HEK 293T, one of the HEK variants used in the present study, includes a coding region for the SV40 Large T-antigen, which promotes efficient replication and expression of transfected plasmids (Nettleship et al., 2015). To measure tau aggregation after plasmid transfection, a HEK variant expressing YFP/CFP-tagged tau fragments was used. Known for their use in fluorescence resonance energy transfer (FRET) analysis, YFP/CFP HEK constructs express cyan- and yellow-emitting variants of green fluorescent protein, a common marker of protein expression (Holmes et al., 2014; Shimozono and Miyawaki, 2008). When stimulated by UV light, unpaired CFP emits light at a characteristic wavelength, as does the YFP/CFP pair; the difference in intensity between the two wavelengths can be used to measure tau aggregation (Tadross et al., 2009).

## 2. Protocols

### 2.1. Transfection

Widely used in studies of protein expression, transfection involves the introduction of nucleic acids into eukaryotic host cells. Methods of transfection belong to three main groups: chemical, viral, and physical. Of the chemical methods, calcium phosphate transfection, polyethylenimine (PEI) transfection, and lipofection are most widely used. In calcium phosphate-based transfection, saline solution containing phosphate ions is combined with a solution of calcium chloride and nucleic acids, the resultant precipitate is added to cell culture, and target cells take up target nucleic acids. In polyethylenimine (PEI) transfection, nucleic acids bind to cationic PEI polymers, which are then taken up by the target cell. In lipofection, negatively charged nucleic acids are surrounded by positively charged liposomes, which merge with cell membranes and deliver the nucleic acids to the cell. Of the viral methods, custom adenoviruses and lentiviruses

are commonly used to introduce target DNA into cell culture. Physical methods such as electroporation and sonoporation, which use electric pulses and ultrasonic waves, respectively, to transiently increase the permeability of cell membranes, are also commonly used, although these protocols require specialized machines (ThermoFisher).

In the present study, lipofection was used to introduce plasmids and siRNA into BV2 and HEK 293T cells. Before transfection, BV2 and HEK 293T cells were grown in cell culture plates (10 mL of cellular media, 100 mL plate) and passed to a new plate once every five days. To harvest HEK 293T cells, 5 mL of 0.05% Trypsin-EDTA was added to the cell culture plate, and the plate was incubated for five minutes at 37° C. To harvest BV2 cells, a cell scraper was used to remove cells from the cell culture plate. Contents of the cell culture plate were then transferred to a 15 mL screw-top tube and centrifuged for 4 minutes at 200 rpm. After removal of supernatant, the remaining cell pellet was resuspended in 12 mL of media and seeded in a 12 well plate. After 2-3 days, cells reached 80% confluence (roughly 3 x $10^5$ cells per well) and were transfected according to the following protocols.

**2.1.1. Plasmid**

Wholly separate from chromosomal DNA, plasmids are small, circular DNA molecules capable of self-replication within a cellular host. As expression vectors, plasmids are used to introduce target genes into host cells and promote expression of desired proteins (Monroe). In the present study, two plasmids were purchased from AddGene, one specific to RNF114 (#58295), containing myc and histidine (his) tags, and another specific to NF-κB (#23288). To transfect plasmids in cell culture, 500 µL of Opti-MEM medium was combined with 10 µL of Lipofectamine 3000 in a 1 mL tube, and 500 µL of Opti-MEM medium was combined with 20 µL of P3000 reagent and 10 µg of plasmid DNA in another 1 mL tube. These solutions were added together, thoroughly mixed,

and allowed to incubate for a period of 15 minutes at room temperature. After incubation, 100 μL of the combined solution was added to each of 10 wells in a 12 well plate, with the remaining 2 wells left blank to serve as a control. Cells were harvested after two days according to the methods above, centrifuged for 4 minutes at 200 rpm, and resuspended in 100 uL of lysis buffer. After lysis, 1 uL of 100x Halt protease inhibitor was added to the solution to limit protein degradation.

**2.1.2. RNAi**

Used to suppress expression of target genes, RNA interference (RNAi) describes an endogenous cellular process in which siRNA duplexes neutralize mRNA transcripts, inhibiting translation and ultimate expression of target DNA. Conserved across eukaryotes, RNAi pathways rely on two kinds of RNA molecules - microRNA (miRNA) and small interfering RNA (siRNA), Upon initiation of RNAi, endogenous Dicer enzyme cleaves double-stranded RNA (dsRNA) into shorter double-stranded fragments of siRNA, which are then separated into passenger and guide strands. After degradation of the passenger strand, the guide strand merges with the RNA-induced silencing complex (RISC), and post-transcriptional silencing of a target gene takes place (NCBI).

In the present study, a set of four siRNA duplexes (3 experimental, 1 scrambled control) was purchased from OriGene and used to suppress expression of RNF114 in BV2 and HEK 293T cells. To transfect a siRNA duplex in cell culture, 100 μL of Opti-MEM medium was combined with 6 μL of Lipofectamine RNAiMAX in a 1 mL tube, and 100 μL of Opti-MEM medium was combined with 2 μg of a siRNA duplex in another 1 mL tube. These solutions were added together, thoroughly mixed, and allowed to incubate for a period of 15 minutes at room temperature. After incubation, 100 μL of the combined solution was added to two wells in a 12 well plate, and this process was repeated for the other 3 duplexes, with the remaining 4 wells left blank to serve as a control. Cells were harvested after two days, centrifuged for 4 minutes at 200 rpm, and resuspended

in 100 μL of lysis buffer. After lysis, 1 μL of 100x Halt protease inhibitor was added to each solution to limit protein degradation.

**2.2. Western Blot**

Commonly used in studies of protein expression, western blots allow researchers to separate target proteins from a complex mixture of cellular products and compare expression of target proteins between cell samples (Mahmood and Yang, 2012; ThermoFisher). Western blotting relies on three principles: separation of proteins by size through gel electrophoresis, transfer of separated proteins to a solid membrane, and labeling of target proteins using specific primary and secondary antibodies (Taylor and Posch, 2008). To quantify relative protein expression, ImageJ (imagej.nih.gov) was used to analyze scanned western blots and compare expression of target proteins to loading control (beta-actin) in each well. The following western blot protocol was conducted over three consecutive days.

On the first day, cells were lysed, and the concentrations of protein in lysates were measured using a bicinchoninic acid (BCA) assay. Using these concentrations, the volumes of lysate needed to run 20-30 μg of protein in each well of the gel were calculated and transferred to a new tube, and the volume in each tube was brought up to a final volume of 10 μL using lysis buffer. Next, these solutions were combined with 10 μL of SDS-BME (98% SDS-PAGE, 2% β-mercaptoethanol) and boiled for 10 minutes. Solutions were then loaded into a 15-well NuPAGE 4-12% Bis-Tris Gel (immersed in 1x MOPS-SDS in an Invitrogen Mini Gel Tank), and gel electrophoresis was run at 80 V for 15 minutes and 130 V for 60 minutes. After gel electrophoresis, the gel was placed on an iBolt 2 Mini Stack and proteins were transferred to the iBlot membrane using the following protocol: 20 V for 1 minute, 23 V for 4 minutes, and 25 V for 2 minutes. After transfer, the blot was rinsed with TBS three times and incubated in blocking buffer for 30 minutes.

After block, the blot was incubated in 2 mL of a primary antibody mixture (1 mL TBS, 1 mL blocking buffer, rabbit RNF114 primary and mouse NF-κB primary at 1:500 dilution), and incubated overnight at 4° C.

On the second day, the blot was removed from the primary antibody mixture and rinsed in TBS four times. The blot was then incubated in a secondary antibody mixture (5 mL TBS, 5 mL blocking buffer, anti-rabbit 800 nm fluorescent antibody and anti-mouse 690 nm fluorescent antibody at 1:10,000 dilution) for one hour. After incubation in secondary antibody, blots were scanned at 700 and 800 nm in a LI-COR Odyssey florescent imaging machine. After the initial scan, the blot was rinsed with TBS three times and incubated in blocking buffer for 30 minutes. To label protein load, a measure of the amount of protein in each well, the blot was incubated in 2 mL of a primary antibody mixture (1 mL TBS, 1 mL blocking buffer, mouse beta-actin primary at 1:500 dilution), and incubated overnight at 4° C.

On the third day, the blot was removed from the primary antibody mixture and rinsed in TBS four times. The blot was then incubated in a secondary antibody mixture (5 mL TBS, 5 mL blocking buffer, anti-mouse 690 nm fluorescent antibody at 1:10,000 dilution). After incubation in secondary antibody, blots were scanned at 700 nm in a LI-COR Odyssey florescent imaging machine. Scans from each day were analyzed and compared using the following ImageJ protocol. Each lane of the blot was traced with the rectangle tool, and a plot of relative density was created. Peaks were then traced during the line tool, the area of the marked region was measured using the wand tool, and the Label Peaks function was used to calculate percent of total area. In Excel, measured expression of RNF114 and NF-κB was normalized to expression of beta-actin (a measure of protein load) in each well, and experimental groups were compared using a two-sample t test.

**2.3. Immunohistochemistry (IHC)**

In the study of neurodegenerative diseases, immunohistochemical techniques are used to visualize density and distribution of biomarkers and target proteins in post-mortem brain tissue (Coons et al., 1942). Based on the principle of antibody-antigen interaction, IHC allows for highly specific labeling of target proteins (ThermoFisher). In the present study, IHC was used to label RNF114 in CTE and AD post-mortem brain tissue. The following protocol was conducted over two consecutive days.

On the first day, tissue sections from the frontal cortices of individuals with CTE and AD were retrieved from storage and rinsed five times in 0.1 M Phosphate Buffer (PB) to remove cryoprotectant. To eliminate endogenous peroxidase activity, tissue sections were incubated for 15 minutes at room temperature in 3% $H_2O_2$ (30% stock diluted 10x with PB) and then rinsed five times in 0.1 M PB. Tissue fragments were then incubated in blocking buffer (2.5 mL of Tris-Buffered Saline (TBS), 2.5 mL of Avidin, 0.1% Triton-X, 8% normal goat serum) for 45 minutes at 4° C, then rinsed 3 times with TBS. Next, tissue sections were incubated overnight at 4° C in a primary antibody mixture (1:200 RNF114 primary antibody, 50 µg/ml Biotin, and 2% NGS in TBS).

On the second day, sections were incubated in a secondary antibody mixture (1:200 biotinylated secondary antibody and 2% NGS in TBS) for one hour at 4° C, then rinsed four times in TBS. During incubation in secondary, ABC solution (Vector Labs) was prepared (1 drop of solution A and 1 drop of solution B per 2.5 mL of TBS) and this solution was put on ice for thirty minutes. Tissue sections were then removed from secondary, rinsed four times in TBS, and incubated in ABC solution for one hour at 4° C. After incubation in ABC, DAB solution was prepared (one 3,3′-Diaminobenzidine (DAB) tablet and one urea hydrogen peroxide tablet in 10

mL TBS), and tissue sections were stained for ten minutes at room temperature, then rinsed four times in TBS. Tissue sections were then mounted on slides and dried overnight. The next day, slides were immersed in deionized water for three minutes, 70% ethanol for three minutes, 95% ethanol for three minutes (twice), 100% ethanol for three minutes (twice), and Histoclear for three minutes (three times), coverslips were affixed to slides, and staining patterns were observed under a microscope.

**2.4. Immunocytochemistry (ICC)**

Like IHC, immunocytochemistry uses the principle of antibody-antigen interactions to visualize the distribution of proteins and biomarkers within a cell sample. When viewed under a fluorescent microscope, immunohistochemical staining techniques allow researchers to determine where target proteins are expressed within a cell. In the present study, ICC was used to visualize expression of RNF114 and NF-κB after transfection of plasmids in BV2 cells grown on coverslips. The following protocol was conducted over two consecutive days.

On the first day, cell media was removed from each well, and cells were fixed with a 2% paraformaldehyde solution for 30 minutes. Four coverslips were removed and rinsed five times with PBS+, a mixture of phosphate-buffered saline (PBS) and 0.5% normal horse serum. After the first and second rinse, coverslips were lifted with forceps to remove excess paraformaldehyde from under the coverslip. Coverslips were then incubated in blocking buffer (1% BSA, 5% normal horse serum and 0.05% Triton-100 in PBS) for 30 minutes at room temperature and rinsed three times with PBS+ after block. After this wash, coverslips were removed and placed, cell side up, on the lid of a tray wrapped in parafilm, then flipped over onto 100 μL of a primary antibody solution (1:250 dilution in blocking buffer) and incubated overnight at 4° C.

On the second day, coverslips were rinsed four times with PBS+, placed, cell side up, on the lid of a tray wrapped in parafilm, then flipped over onto 100 µL of a secondary antibody solution (1:100 dilution in blocking buffer) and incubated for one hour at room temperature. After a second set of PBS+ washes, coverslips were mounted on slides using vectashield mounting media and dried overnight. An Olympus BX51 fluorescent microscope (20x magnification) was used to image slides at 488 nm (rabbit-based primary antibodies) and 568 nm (to highlight mouse- and goat-based primary antibodies).

**2.5. Fluorescence resonance energy transfer (FRET)**

Used primarily to detect molecular interactions, fluorescence resonance energy transfer (FRET) describes the distance-dependent transfer of energy between two fluorescent molecules, or chromophores, through non-radiative bonding (Lamond). For FRET to occur, the donor and acceptor molecules must be 10 to 100 ångstroms (1 to 10 nanometers) apart, the emission spectrum of the donor molecule must overlap the absorption spectrum of the acceptor molecule, and the transition dipole configuration of each molecule must be parallel (Hussain, 2009). As the efficiency of FRET is equal to $1/(1+(r/R_o)^6)$, where r is the distance between the donor and acceptor molecules and $R_o$ is the distance at which the efficiency of energy transfer is 50%, FRET analysis is capable of detecting extremely small changes in the distance between two molecules. As such, FRET analysis is widely used to study protein aggregation and structure, enzyme kinetics, and gene interactions (Held, 2005).

In the present study, a line of HEK cells expressing YFP/CFP-tagged tau fragments were transfected with an RNF114 plasmid and AD homogenate (Holmes et al., 2014). After transfection, the wells were stimulated with UV light (414 nm) and the relative intensity of cyan (475 nm) and yellow (525 nm) light was measured; a higher proportion of yellow light in the FRET signal

corresponded with a greater degree of tau aggregation. Taylor Pohl, another undergraduate in the Hales lab, grew the YFP/CFP HEK cells, transfected the cells with the plasmids from the present study and AD homogenate, and conducted the subsequent FRET analysis. FRET data was transferred to Excel, and tau aggregation in each condition was compared to control using a two-sample t test.

**2.6. qPCR**

Quantitative real-time PCR (qPCR) allows for measurement of DNA amplification in real time. In qPCR, a fluorescent signal is generated in proportion to the degree of DNA amplification; this signal is highly sensitive and can detect as few as five DNA molecules in ideal conditions (Milstein et al., 2013). In the present study, qPCR was used to verify RNAi knockdown of RNF114 expression in HEK 293T cell culture. An RNF114 gene expression assay was purchased from ThermoFisher (Hs00218782_m1) along with TaqMan™ Fast Advanced Master Mix. The gene expression assay contained a pair of unlabeled PCR primers and a TaqMan probe with a FAM dye label on the 5' end and a non-fluorescent quencher (NFQ) and a minor groove binder (MGB) on the 3' end. The following cDNA-qPCR protocol was conducted over two days.

A 12-well plate of BV2 cells was transfected with four siRNA duplexes specific to RNF114 according to the protocol above. On the first day of the qPCR protocol, these cells were harvested from the plate, transferred to 1.5 mL flip-top tubes, centrifuged at 200 RPM for 4 minutes, resuspended in TBS, then centrifuged at the same settings for a second time. To extract RNA, cells in each flip-top tube were resuspended in 1 mL of Trizol and incubated for 10 minutes at room temperature. Next, 0.2 mL of chloroform was added to each tube, tubes were shaken vigorously for 15 seconds, and tubes were then incubated for 3 minutes at room temperature. Tubes were then centrifuged at 12,000*g* for 15 minutes at 4° C. After centrifugation, the mixture separated into three

phases: a lower red phenol chloroform phase, an interphase, and a colorless upper aqueous phase. Extracted RNA stayed within the upper aqueous phase (roughly 50% of the total volume), and this phase was transferred to a new tube. Next, 500 µL of 100% isopropanol was added to the aqueous phase, samples were incubated for 10 minutes at room temperature, and the tubes were centrifuged at 12,000*g* for 10 minutes at 4° C. After centrifugation, the supernatant was removed from each tube, and the RNA pellet was washed with 1 mL of 75% ethanol (vortex for 15 seconds, centrifuge at 7500*g* for 5 minutes at 4° C). After the ethanol wash, the supernatant was discarded, and the RNA pellet was allowed to dry for 15 minutes. The RNA pellet was then resuspended in 30 µL of RNAase-free water and incubated for 15 minutes at 60° C. Concentration of the RNA samples was measured using a NanoDrop, and the samples were stored at 80° C.

On the second day, cell samples were removed from storage and cDNA was synthesized according to the following protocol. 25 µL of reverse transcriptase solution (5 µL 10x RT buffer, 5 µL random primers, 2 µL 10mM dNTP, 2.5 µL reverse transcriptase, and 10.5 µL DEPC-$H_2O$) was added to 25 µL of diluted RNA. In a Veriti 96-well thermal cycler, the following PCR program was run: 25° C (10 minutes), 37° C (2 hours), 85° C (5 minutes), and 4° C (hold). Synthesized cDNA was diluted 10-fold, and 5 µL of cDNA from each diluted sample was added to the following: 10 µL of TaqMan Universal PCR Master Mix, 1 µL of TaqMan gene expression assay primers, and 4 µL nuclease-free $H_2O$, for a total volume of 20 µL. Two primers were used (RNF114 and HPRT1, a housekeeping gene) and samples were transferred to a 96-well plate in triplicate (10 samples, two primers, 60 wells in total). Next, a Falcon Multiwell qPCR machine was programmed to the following settings - 7500 Fast (96-well), Quantitation, Comparative CT, TaqMan reagents, standard (2 hours), cDNA - and the following PCR program was run: 1 cycle at 20° C (20 seconds), 1 cycle at 95° C (10 minutes), and 40 cycles at 95° C (15 seconds) and 60° C (1 minutes). qPCR

data was transferred to Excel, and expression of RNF114 in the RNAi knockdown condition was compared to control using a two-sample t test.

**2.7. Mechanical Trauma**

Current models of rmTBI require the use of animal models, which can be time- and resource-intensive, or rely on mechanical stretching of cell culture, which fails to model the linear and angular acceleration characteristic of rmTBI. In the present study, we set out to establish a mechanical trauma model that could subject BV2 cells to the linear and angular acceleration involved in traumatic brain injury. While many models were devised and initially tested (vigorous resuspension with a pipette, aeration of resuspended cells, etc.), only agitation of BV2 cell pellets in a vortex machine was found promote a cellular response. The following mechanical trauma protocol was followed for all experiments.

Before each experiment, BV2 cells were grown in a cell culture plate (10 mL of cell media, 100 mL plate) and passed to a new plate once every five days. To harvest the cells, a cell scraper was used to remove cells from the cell culture plate. The contents of the cell culture plate were then transferred to multiple 15 mL screw-top tubes and centrifuged for 4 minutes at 200 rpm. After removal of supernatant, the cell pellet remaining in the tubes was suspended in 1 mL of media and agitated in a vortex machine for a predetermined period of time (5 seconds minimum, 270 seconds maximum). Agitated cells were then seeded in a 12-well or 100 mL culture plate, harvested and lysed at predetermined time intervals, and expression of RNF114 was quantified using the western blot protocol described previously. In addition, cells were examined with a Nikon T51000 microscope at 20x magnification before harvest, to determine average cell density and examine cell morphology.

## Experiments and Results

### 1. Validation of Data from the CTE Insoluble Proteome

As protein deposition is a prominent feature in many neurodegenerative diseases, evaluation of the insoluble proteome can uncover proteins that drive disease pathophysiology. A recent study on the CTE insoluble proteome (Hales et al., 2017) demonstrated many disease-specific changes in protein expression, including a depression of RNF114 expression across all four stages of CTE (-0.58, $p = 0.0028$). To validate the depression of RNF114 expression found in the CTE insoluble proteome and compare endogenous expression of RNF114 and NF-κB in CTE with that of a control sample, the following four experiments were conducted **(Table 1)**.

In the first experiment, post-mortem tissue sections from the frontal cortices of CTE and AD patients were stained using an IHC protocol to visualize expression of RNF114 in CTE and compare localization of RNF114 in CTE with that of AD. However, deposits of RNF114 were not visible in either the AD or the CTE cases after IHC staining. As such, western blotting was used in subsequent experiments to measure expression of RNF114 and NF-κB.

In the second experiment, homogenates from the frontal cortices of six individuals with CTE - 8965, 7748, 9580, 7738, 6605, and 8473 - were compared to homogenates from six individuals without CTE pathology - E06-45, A87-50, OS03-299, A93-03, OS03-390, and E08-101 - and endogenous expression of RNF114 was measured through western blotting. Relative to loading control (beta-actin), mean expression of RNF114 in the control group ($0.342 \pm 0.0582$) was significantly higher than mean expression of RNF114 in the CTE group ($0.219 \pm 0.0435$, $p = 0.002$), suggesting that expression of RNF114 is significantly reduced in CTE **(Figure 2)**. As these samples came from a variety of patients, brain regions, and stages, this result validates the

depression of RNF114 expression found through quantitative proteomic evaluation of the CTE insoluble proteome.

In the third experiment, unmodified BV2 cell lysate was compared to homogenate from the frontal cortex of one individual with CTE (8965) through western blotting to compare expression of RNF114 and NF-κB between cohorts. This comparison found that expression of RNF114 was depressed in CTE (0.1455x), while expression of NF-κB was increased (13.5x). However, this comparison did not reach significance (n = 1 for each group). In the fourth experiment of the validation series, the sample size for each group was increased, and seven samples of unmodified BV2 cell lysate were compared to seven samples of homogenate from the frontal cortex of an individual with CTE (8965) through western blotting. This comparison supported the results of the third experiment, finding that expression of RNF114 was depressed in CTE (0.21x, $p = 0.0001$), while expression of NF-κB was increased (3.07x, $p < 0.0001$) **(Figure 3)**. These results support the hypothesis that RNF114 serves as a negative regulator of NF-κB and suggest that depression of RNF114 expression may lead to increased expression of NF-κB.

**Table 1. Validation of Data from the CTE Insoluble Proteome (all values are relative to loading control)**

| **Insoluble Proteome** | **CTE1-CTL** | **CTEII-III-CTL** | **CTEIV -CTL** | **CTE11-CTL** | **p-value** |
|---|---|---|---|---|---|
| *RNF114* | -0.6523219 | -0.585807 | -0.5201289 | -0.5800645 | 0.00287124 |
| **Experiment 2** | **Average** | **SD** | **Multiple of Control** | **p-value** | **t-value** |
| *CTE* | 0.21908911 | 0.04352149 | 0.64098419 | 0.002 | 4.1377 |
| *Control* | 0.34180111 | 0.05816496 | | | |
| **Experiment 3** | **NF-κB** | **RNF114** | | | |
| *8965 (CTE)* | 0.26599365 | 0.04984331 | | | |
| *BV2 (Control)* | 0.01965872 | 0.34247177 | | | |
| *Multiple* | 13.5305706 | 0.1455399 | | | |
| **Experiment 4** | **Average** | **SD** | **Multiple of Control** | **p-value** | **t-value** |
| *RNF114 - BV2* | 2.63898392 | 0.87127653 | | | |
| *RNF114 - 8965* | 0.55787828 | 0.27199814 | 0.21139889 | 0.0001 | 10.5987 |
| *NF-kB - BV2* | 0.53982316 | 0.2430013 | | | |
| *NF-kB - 8965* | 1.65658831 | 0.19514674 | 3.0687611 | <0.0001 | 9.1993 |

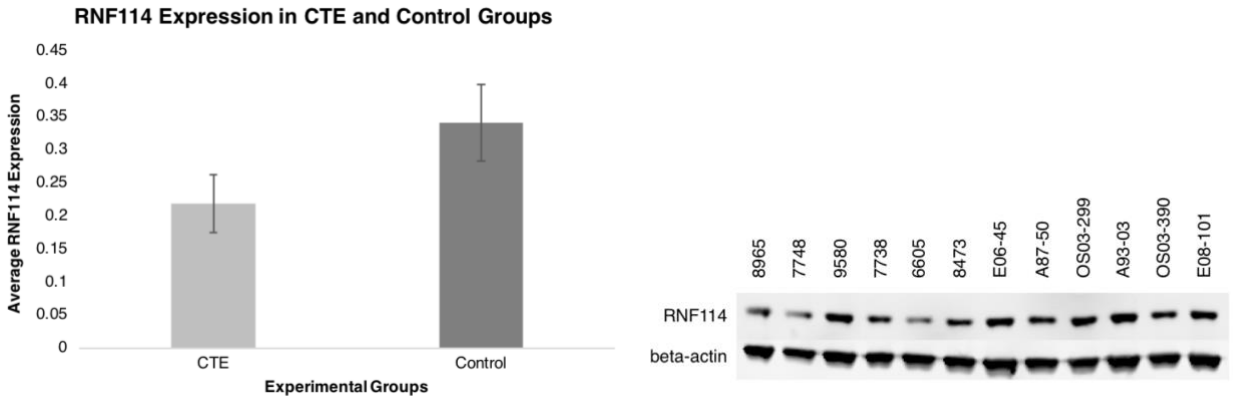


**Figure 2. Depression of RNF114 expression in a sample of CTE patients**

Homogenates from the frontal cortices of six individuals with CTE (8965, 7748, 9580, 7738, 6605, and 8473) were compared to homogenates from the frontal cortices of from six individuals without CTE (E06-45, A87-50, OS03-299, A93-03, OS03-390, and E08-101) through western blotting (right). Relative to loading control, mean expression of RNF114 in the control group ($0.342 \pm 0.0582$) was significantly higher than mean expression of RNF114 in the CTE group ($0.219 \pm 0.0435$, $p = 0.002$) (left).

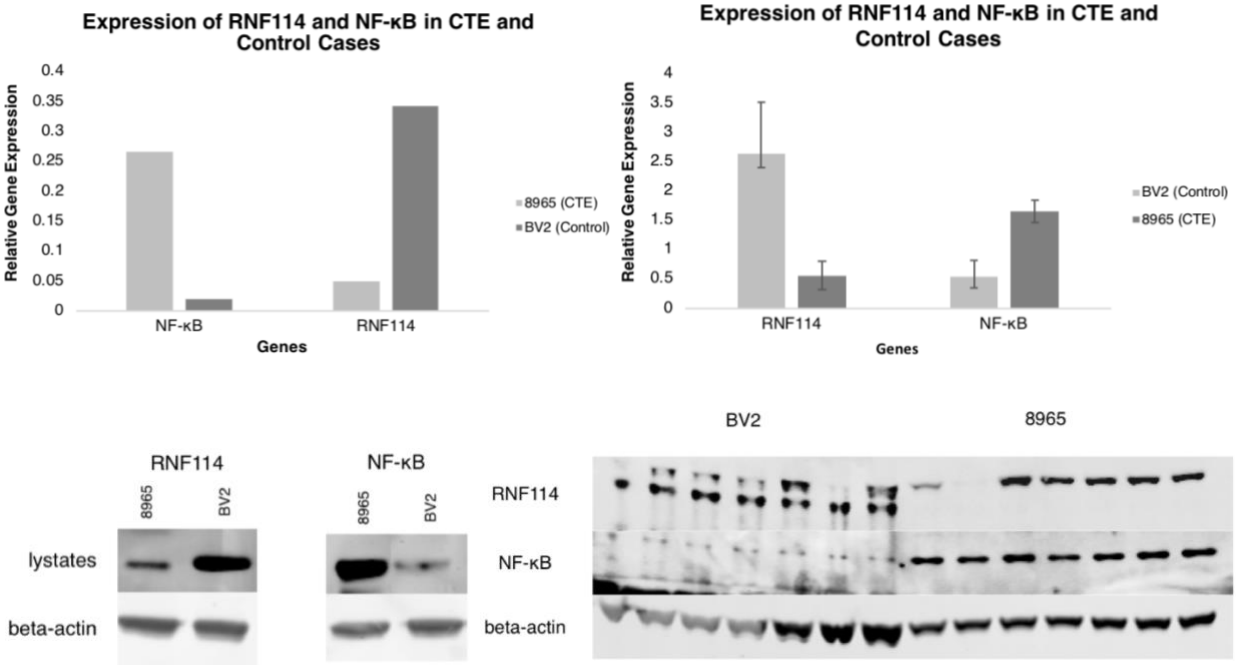


**Figure 3. Expression of RNF114 and NF-κB in a CTE patient compared to control**

Unmodified BV2 cell lysate was compared to homogenate from the frontal cortex of one individual with CTE (8965) through western blotting (bottom left). Expression of RNF114 was found to be depressed in CTE (0.1455x), while expression of NF-κB was found to be increased (13.5x) (upper left). To study this relationship further, seven samples of unmodified BV2 cell lysate were compared to seven samples of CTE homogenate (8965) through western blotting (bottom right). This comparison supported the results of the previous experiment, finding that expression of RNF114 was depressed in CTE (0.21x, $p = 0.0001$), while expression of NF-κB was increased (3.07x, $p < 0.0001$) (upper right).

**2. Transfection of Plasmid Over-Expression Constructs**

To measure the effect of up-regulation of RNF114 in BV2 and HEK 293T cells on expression of NF-κB and aggregation of tau, the following four experiments were conducted, each involving the transfection of a 12-well plate of cells with plasmid over-expression constructs. Protein expression was measured using western blotting, and tau aggregation was measured through FRET analysis in a HEK 293T YFP/CFP tau biosensor line **(Table 2)**.

In the first experiment, BV2 cells were transfected with an RNF114 plasmid (8 wells transfected, 4 wells control), harvested after a two-day incubation period, and changes in expression of RNF114 were measured though western blotting. After transfection, expression of RNF114 was increased by 2.22x ($p = 0.0054$) and expression of NF-κB was decreased by 0.40x ($p = 0.016$). In the second experiment, BV2 cells were transfected with an NF-κB plasmid (8 wells transfected, 4 wells control), harvested after a two-day incubation period, and changes in expression of NF-κB were measured though western blotting. After transfection, expression of NF-κB was increased by 3.81x ($p = 0.0049$) and expression of RNF114 was increased by 8.15x ($p = 0.0083$). In these experiments, up-regulation of RNF114 led to down-regulation of NF-κB, and up-regulation of NF-κB was followed by a proportionate increase in RNF114 expression; these results provide further support for the hypothesis that RNF114 serves as a negative regulator of NF-κB in BV2 cells **(Figure 4)**.

In the third experiment, an ICC protocol was used to visualize localization of target proteins in transfected BV2 cell culture. BV2 cells were grown on coverslips, transfected with RNF114 and NF-κB plasmids (5 wells each), and harvested after a two-day incubation period. Using the ICC protocol detailed previously, four coverslips (1, 2, 3 - RNF114, 4 - NF-κB) were stained for RNF114 (1 and 4), NF-κB (4), myc (1 and 3) and histidine (2 and 3) tags, and cell nuclei (Hoescht,

all 4) and mounted on slides. When observed under a fluorescent microscope, perinuclear and cytoplasmic deposits of RNF114 and NF-κB were observed **(Figure 5)**.

In the fourth experiment, FRET analysis was used to measure aggregation of tau in a HEK 293T YFP/CFP tau biosensor line after transfection with an RNF114 plasmid. HEK 293T cells expressing YFP/CFP-tagged tau fragments were transfected with an RNF114 plasmid (9 wells), with the remaining 2 wells left blank to serve as a control. Additionally, AD homogenate was added in 5 plasmid wells to determine whether RNF114 would require the presence of preformed tau seeds to promote aggregation. As described previously, cells were stimulated with UV light, and a FRET signal was measured, corresponding to aggregation of tau. The difference between aggregation in the control condition ($0.34 \pm 0.0565$) and aggregation in the plasmid condition ($0.47 \pm 0.124$) was found to be statistically insignificant ($p = 0.2481$), while the difference between aggregation in the control condition and aggregation in the plasmid/homogenate condition ($1.284 \pm 0.203$) was found to be statistically significant ($p = 0.0016$). These results suggest that RNF114 up-regulation alone does not lead to an increase in tau aggregation, but rather that introduction of AD homogenate promotes increased aggregation of tau **(Figure 6)**. This finding may provide additional support for the template-based hypothesis of tau aggregation (Kfoury et al., 2012).

| Table 2. Transfection of Plasmid Over-Expression Constructs (all values are relative to loading control) | | | | | |
|---|---|---|---|---|---|
| **Experiments 1 and 2** | **Average** | **SD** | **Multiple** | **p-value** | **t-value** |
| *RNF114* | 2.19495508 | 0.18013492 | 2.21860443 | 0.0054 | 7.2421 |
| *RNF114 (NFkB)* | 0.39392503 | 0.13663996 | 0.39816934 | 0.016 | 4.886 |
| *NFkB* | 3.77374736 | 0.19497143 | 3.81440726 | 0.0049 | 14.22 |
| *NFkB (RNF114)* | 8.06752904 | 0.64610091 | 8.15445191 | 0.0083 | 10.94 |
| **Experiment 4** | **Average** | **SD** | **Multiple** | **p-value** | **t-value** |
| *Control* | 0.34 | 0.05656854 | | | |
| *RNF114* | 0.47 | 0.12409674 | 1.38235294 | 0.2481 | 1.3508 |
| *RNF114 + AD* | 1.284 | 0.2025863 | 3.77647059 | 0.0016 | 6.1670 |

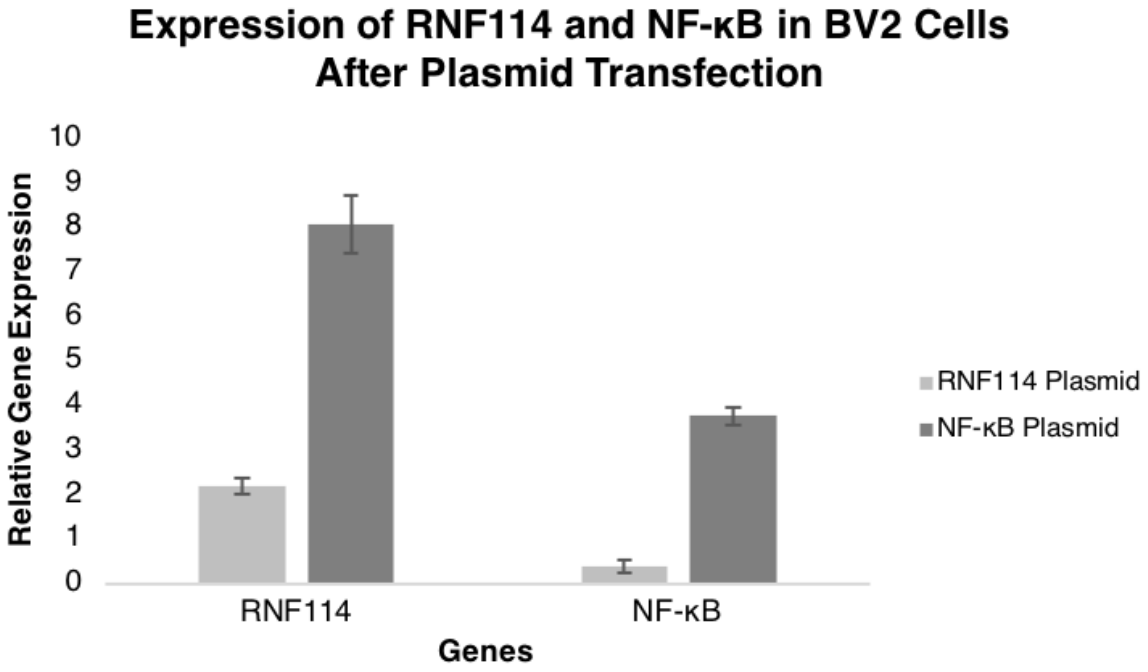


**Figure 4. Transfection of BV2 cells with plasmid over-expression constructs**

BV2 cells were transfected with an RNF114 plasmid, harvested after a two-day incubation period, and changes in expression of RNF114 were measured though western blotting. After transfection, expression of RNF114 was increased by 2.2x ($p = 0.0054$) and expression of NF-κB was decreased by 0.39x ($p = 0.016$). In the second experiment, BV2 cells were transfected with a plasmid specific to NF-κB, harvested after a two-day incubation period, and changes in expression of NF-κB were measured though western blotting. After transfection, expression of NF-κB was increased by 3.77x ($p=0.0049$) and expression of RNF114 was increased by 8.07x ($p=0.0083$)

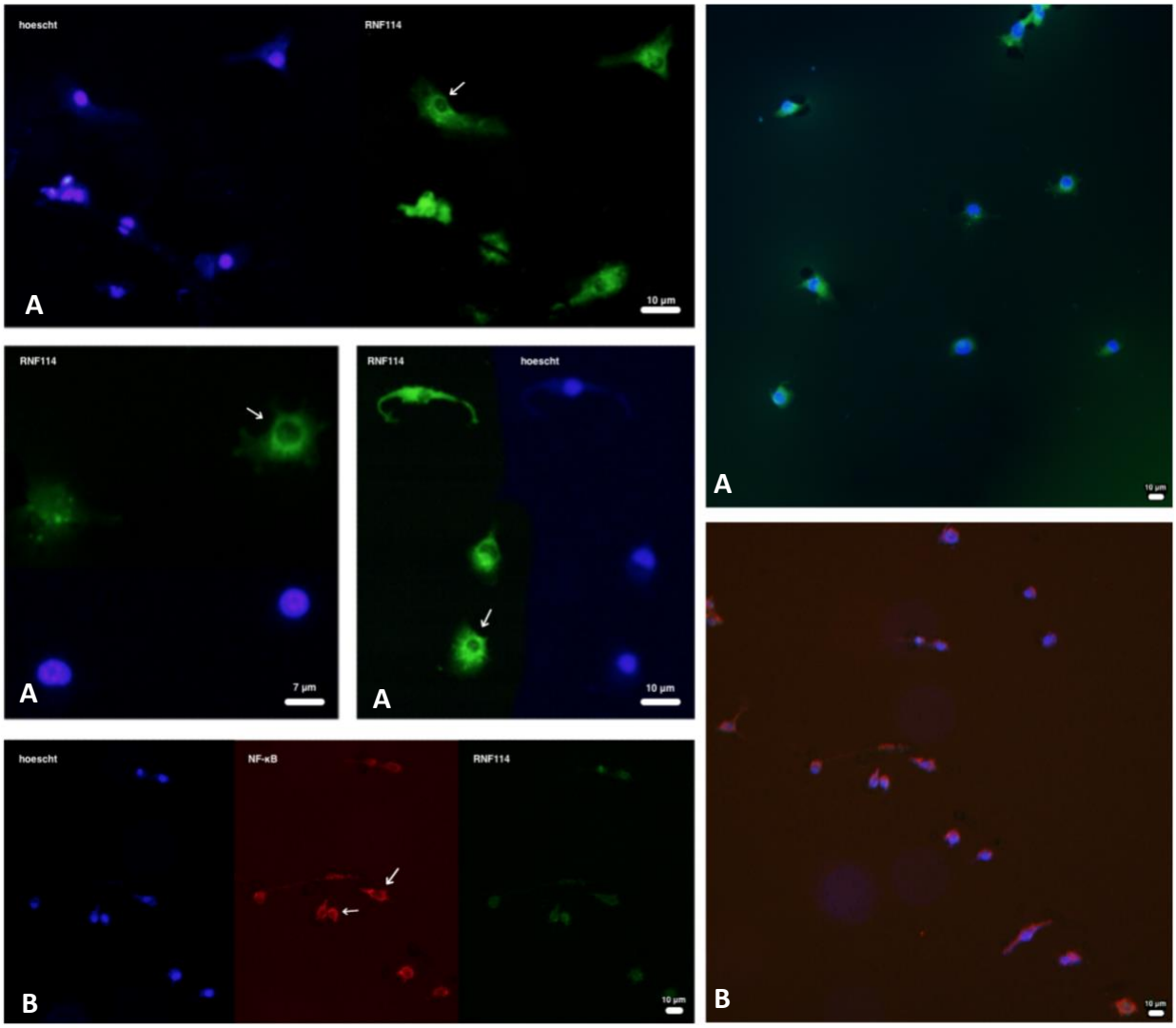


**Figure 5. ICC staining of BV2 cells after plasmid transfection**

BV2 cells were grown on coverslips, transfected with plasmids specific to RNF114 and NF-κB and harvested after a two-day incubation period. Using an ICC protocol, four coverslips (RNF114 - 1, 2, 3, NF-κB - 4) were stained for RNF114, NF-κB and cell nuclei (Hoescht), mounted on slides, and examined under an Olympus BX51 fluorescent microscope at 20x magnification. **(A)** Labeling cell nuclei (Hoescht) and RNF114 after transfection with the RNF114 plasmid revealed diffuse perinuclear and cytoplasmic deposits of RNF114. **(B)** Labeling cell nuclei, NF-κB, and RNF114 after transfection with a plasmid specific NF-κB revealed dense perinuclear and cytoplasmic deposits of NF-κB, accompanied by diffuse deposits of RNF114.

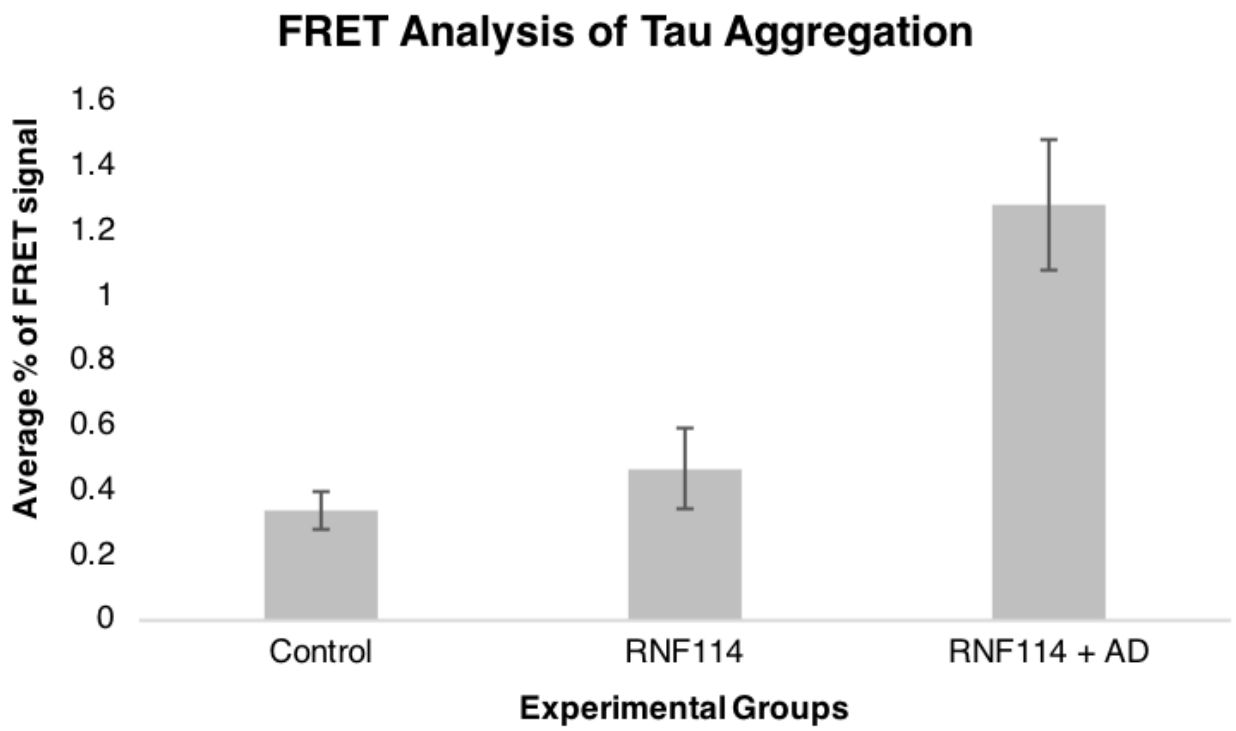


**Figure 6. Measuring tau aggregation after transfection through FRET analysis**

HEK 293T cells expressing YFP/CFP-tagged tau fragments were transfected with an RNF114 plasmid and plasmid plus AD homogenate, with two wells left blank as a control. Cells were stimulated with UV light, and a FRET signal, corresponding to aggregation of tau, was measured. The difference between aggregation in the control condition (0.34 ± 0.0565) and aggregation in the plasmid condition (.47 ± 0.124) was found to be statistically insignificant ($p = 0.2481$), while the difference between aggregation in the control condition and aggregation in the plasmid/homogenate condition (1.284 ± 0.203) was found to be statistically significant ($p = 0.0016$).

### 3. Transfection of siRNA Duplexes

While plasmid over-expression in BV2 cell culture allowed for exploration of the relationship between expression of RNF114 and expression of NF-κB, knockdown of RNF114 expression would better model the depression of RNF114 expression found in the insoluble proteome of CTE. To measure the effect of RNF114 knockdown on expression of NF-κB, the following three RNAi experiments were conducted, each involving the transfection of a 12-well plate with four siRNA duplexes (three active, one scramble control) **(Table 3)**.

In the first experiment, four siRNA duplexes were transfected in duplicate in a plate of BV2 cells (8 wells transfected, 4 wells control), harvested after a two-day incubation period, lysed, and changes in expression of RNF114 were measured though western blotting. Relative to loading

control (beta-actin), the difference between RNF114 expression in the control condition (1.005 ± 0.141) and RNF114 expression in the RNAi condition (1.036 ± 0.39) did not reach statistical significance, suggesting that knockdown of RNF114 expression did not occur **(Figure 7)**.

In the second experiment, BV2 cells were replaced with HEK 293T cells to improve transfection efficiency, and green fluorescent protein (GFP) was used to verify success of the transfection protocol. Four siRNA duplexes were transfected in duplicate in a plate of HEK 293T cells (8 wells transfected, 2 wells GFP, 2 wells control), harvested after a three-day incubation period, lysed, and changes in expression of RNF114 were measured though western blotting. Relative to loading control (beta-actin), the difference between RNF114 expression in the control condition (0.982 ± 0.615) and RNF114 expression in the RNAi condition (1.676 ± 0.855) did not reach statistical significance, suggesting that knockdown of RNF114 expression did not occur **(Figure 8)**.

As proteins can persist for days within the cell, complicating attempts to measure knockdown through western blotting, qPCR was used in the third experiment to measure knockdown of mRNA in real time. Four siRNA duplexes were transfected in duplicate in a plate of HEK 293T cells (8 wells transfected, 4 wells control), and harvested after a two-day incubation period. As described previously, mRNA was extracted and purified, cDNA was synthesized, and qPCR was used to verify knockdown of RNF114 expression in real time. Compared to the negative control condition, siRNA duplexes #1 and #3 caused a statistically significant depression of mRNA synthesis ($p = 0.0021$ and 0.0001, respectively), while the scramble duplex (negative control) and siRNA duplex #2 did not cause a statistically significant depression of mRNA synthesis ($p = 0.8836$ and 0.283, respectively). These results suggest that the RNAi protocol used in prior experiments successfully knocked down synthesis of mRNA, but that this knockdown was not reflected in protein expression within the period of incubation.

| Table 3. Transfection of siRNA Duplexes (all values are relative to loading control) | | | | |
|---|---|---|---|---|
| **Experiment 1** | **Average** | **SD** | **p-value** | **t-value** |
| RNAi | 1.03598161 | 0.39010946 | 0.9673 | 0.0427 |
| Control | 1.00543238 | 0.1413871 | | |
| **Experiment 2** | **Average** | **SD** | **p-value** | **t-value** |
| *RNAi* | 1.67601069 | 0.85520804 | 0.329 | 1.0491 |
| *Control* | 0.98191743 | 0.61468367 | | |
| **Experiment 3** | **% of Control** | **SD** | **p-value** | **t-value** |
| *RNA #1* | 41.1958309 | 6.16602842 | 0.0001 | 7.2315 |
| *RNA #2* | 123.890098 | 12.771637 | 0.283 | 2.5617 |
| *RNA #3* | 49.3348546 | 23.4984955 | 0.0021 | 4.112 |
| *Scramble Control* | 101.600418 | 17.9385656 | 0.8836 | 0.1502 |

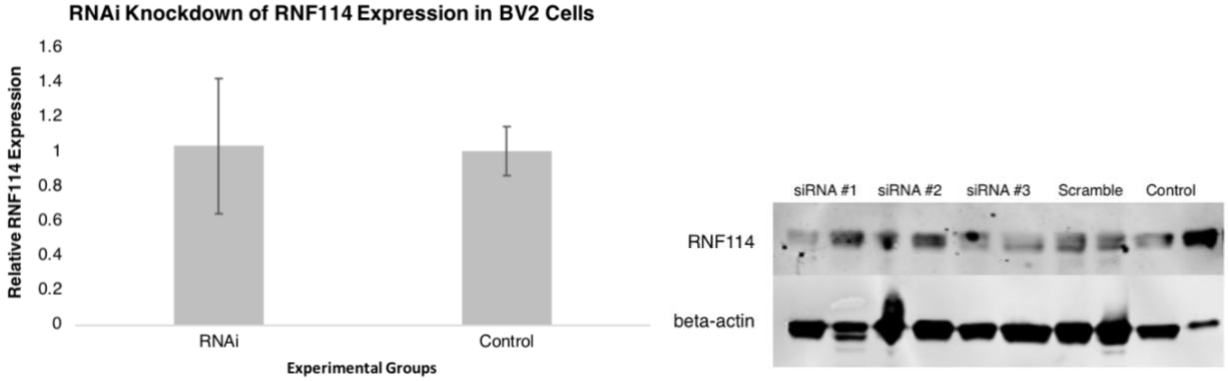


**Figure 7. RNAi-mediated knockdown of RNF114 expression in BV2 cells**

Four siRNA duplexes were transfected in duplicate in a plate of BV2 cells, harvested after a two-day incubation period and lysed. Changes in expression of RNF114 were measured though western blotting (right). Relative to protein load, the difference between RNF114 expression in the control condition (1.005 ± 0.141) and RNF114 expression in the RNAi condition (1.036 ± 0.39) did not reach statistical significance (left). These results suggest that knockdown of RNF114 expression was not successful.

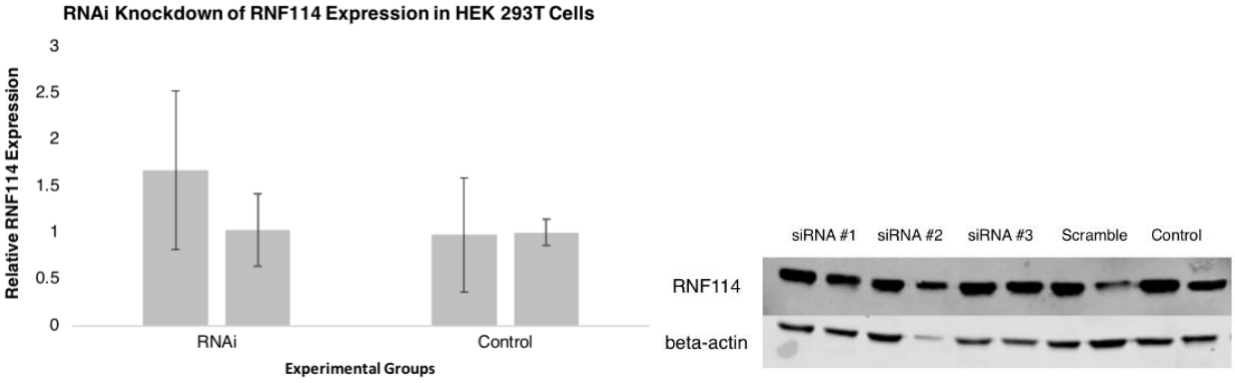


**Figure 8. RNAi-mediated knockdown of RNF114 expression in HEK 293T cells**

Four siRNA duplexes were transfected in duplicate in a plate of HEK 293T cells (8 wells transfected, 2 wells GFP, 2 wells control), harvested after a three-day incubation period, and lysed. Changes in expression of RNF114 were measured though western blotting (right). Relative to protein load, the difference between RNF114 expression in the control condition (0.982 ± 0.615) and RNF114 expression in the RNAi condition (1.676 ± 0.855) did not reach statistical significance (left). These results suggest that knockdown of RNF114 expression was not successful.

**4. Modeling Mechanical Trauma in BV2 Cell Culture**

As described previously, cellular trauma models that accurately capture the linear and angular acceleration characteristic of rmTBI have not previously been described in the literature. Additionally, a cellular repetitive trauma model could provide insight into the effect of rmTBI on expression of RNF114 and NF-κB. To create a simple model of mechanical trauma in BV2 cell culture and measure the effect of this intervention on expression of RNF114 in BV2 cell culture, the following three experiments were conducted **(Table 4)**.

In the first experiment, candidate models of mechanical trauma were devised and tested using BV2 cells. Cells were separated into one of six experimental conditions: control, vigorous resuspension with pipette (90 seconds), aeration of solution (90 seconds), and agitation of cells in a vortex machine (5 seconds, 10 seconds, and 30 seconds). Each experimental group was plated in 4 wells (24 wells total), then photographed, harvested, and lysed at 6, 24, 48, and 96 hours post-intervention. Of these conditions, agitation of cells in a vortex machine for thirty seconds was found to correlate with an increase in RNF114 expression after intervention - 3.98x at 6 hours and 3.28x at 96 hours **(Figure 9)**.

In the second experiment, the duration of agitation was increased threefold, and the effect of this intervention on RNF114 expression was measured at four and eight days after initial trauma. BV2 cells were separated into one of two experimental conditions: control and agitation of cells in a vortex machine (90 seconds). Cells were plated after the experiment, then harvested and passed to new plates at four and eight days post-intervention. Through western blotting, a statistically significant increase in RNF114 expression was found at four (5.05x, $p = 0.0109$) and eight (3.17x, $p = 0.0008$) days after initial intervention **(Figure 10)**. These results suggest that in healthy BV2 cells, RNF114 expression is heavily up-regulated after acute trauma and attenuated as time passes.

In the third experiment, a wider variety of durations and incubation periods were tested, and expression of RNF114 was measured for each condition and time point. BV2 cells were separated into one of five experimental conditions: control and vortex (30, 60, 180, 270 seconds), then photographed and harvested at 1, 2, 3, 4, and 8 days after the initial intervention. Qualitative assessment of cell culture suggested that cells exhibited reduced cell density after agitation in a vortex machine; in addition, the morphology of cells in the vortex cohort appeared to differ from that of the control cohort **(Figure 12)**. However, subsequent blotting of cell lysates proved inconclusive. While increased duration of agitation appeared to increase RNF114 expression, the difference between mean RNF114 expression in the control wells and RNF114 expression in each vortex condition (30, 60, 180, 270 seconds) averaged over time (1, 2, 3, and 4 days) did not reach significance ($p = 0.1701, 0.0922, 0.0825, 0.2951$) **(Figure 11)**. While agitation of BV2 cells in a vortex machine may elicit an increased inflammatory response, further studies are needed to establish the efficacy of this method.

| Table 4. Modeling Mechanical Trauma in BV2 Cell Culture (all values are relative to loading control) | | | | | |
|---|---|---|---|---|---|
| **Experiment 1** | **6 Hours** | **24 Hours** | **48 Hours** | **96 Hours** | |
| *Control* | 0.33105636 | 2.79366476 | 0.36986847 | 0.37727527 | |
| *Pipette* | 0.16280926 | 3.3559322 | 0.09566384 | 0.25246057 | |
| *V5* | 0.28383142 | 5.98519924 | 1.00254852 | 0.19695607 | |
| *V10* | 0.46658 | 4.49389514 | 0.26879574 | 0.84297424 | |
| *V30* | 1.31442663 | 3.0813197 | 0.70265115 | 1.23978535 | |
| **Multiple of Control** | **6 Hours** | **24 Hours** | **48 Hours** | **96 Hours** | |
| *Pipette* | 0.49336139 | 1.20284308 | 0.25855091 | 0.66930162 | |
| *V5* | 0.8600952 | 2.1452327 | 2.70959059 | 0.52215288 | |
| *V10* | 1.41387879 | 1.6107151 | 0.72647498 | 2.23482036 | |
| *V30* | 3.98311101 | 1.10441566 | 1.89905717 | 3.28681164 | |
| **Experiment 2** | **RNF114** | **Multiple of Control** | **SD** | **p-value** | **t-value** |
| *Control (4 days)* | 0.79286493 | | 0.5592226 | | |
| *Vortex (4 days)* | 4.01010698 | 5.0577429 | 1.10662237 | 0.0109 | 4.4963 |
| *Control (8 days)* | 1.29257898 | | 0.1440436 | | |
| *Vortex (8 days)* | 4.10138039 | 3.17302111 | 0.27525379 | 0.0008 | 9.0412 |
| **Experiment 3** | **1 Day** | **2 Days** | **3 Days** | **4 Days** | **8 Days** |
| *Control* | 0.5973424 | 0.90163399 | 0.63581405 | 0.98484495 | |
| *V30* | 0.86850829 | 0.84064 | 0.70537784 | 0.54245974 | 0.93311376 |
| *V60* | 1.20065253 | 0.85946265 | 0.9052381 | 0.65077099 | 1.27719001 |
| *V180* | 1.15536232 | 0.8859683 | 1.44126074 | 0.56285566 | 1.19381071 |
| *V270* | 0.71303532 | 0.65552699 | 0.58819988 | 0.75548506 | 1.61559196 |
| **Multiple of Control** | **1 Day** | **2 Days** | **3 Days** | **4 Days** | **8 Days** |
| *V30* | 1.45395386 | 0.93235172 | 1.10940902 | 0.55080725 | 0.93311376 |
| *V60* | 2.00999047 | 0.95322788 | 1.4237466 | 0.66078522 | 1.27719001 |
| *V180* | 1.93417096 | 0.98262523 | 2.266796 | 0.57151703 | 1.19381071 |
| *V270* | 1.19367941 | 0.72704335 | 0.92511306 | 0.76711066 | 1.61559196 |
| **Analysis** | **Average** | **SD** | **p-value** | **t-value** | |
| *Control* | 0.77990885 | 0.19227553 | | | |
| *V30* | 1.12172611 | 0.4081283 | 0.1701 | 1.5292 | |
| *V60* | 1.43717413 | 0.64354649 | 0.0922 | 1.9499 | |
| *V180* | 1.55072918 | 0.73176318 | 0.0825 | 2.0255 | |
| *V270* | 1.26351589 | 0.8262011 | 0.2951 | 1.1215 | |

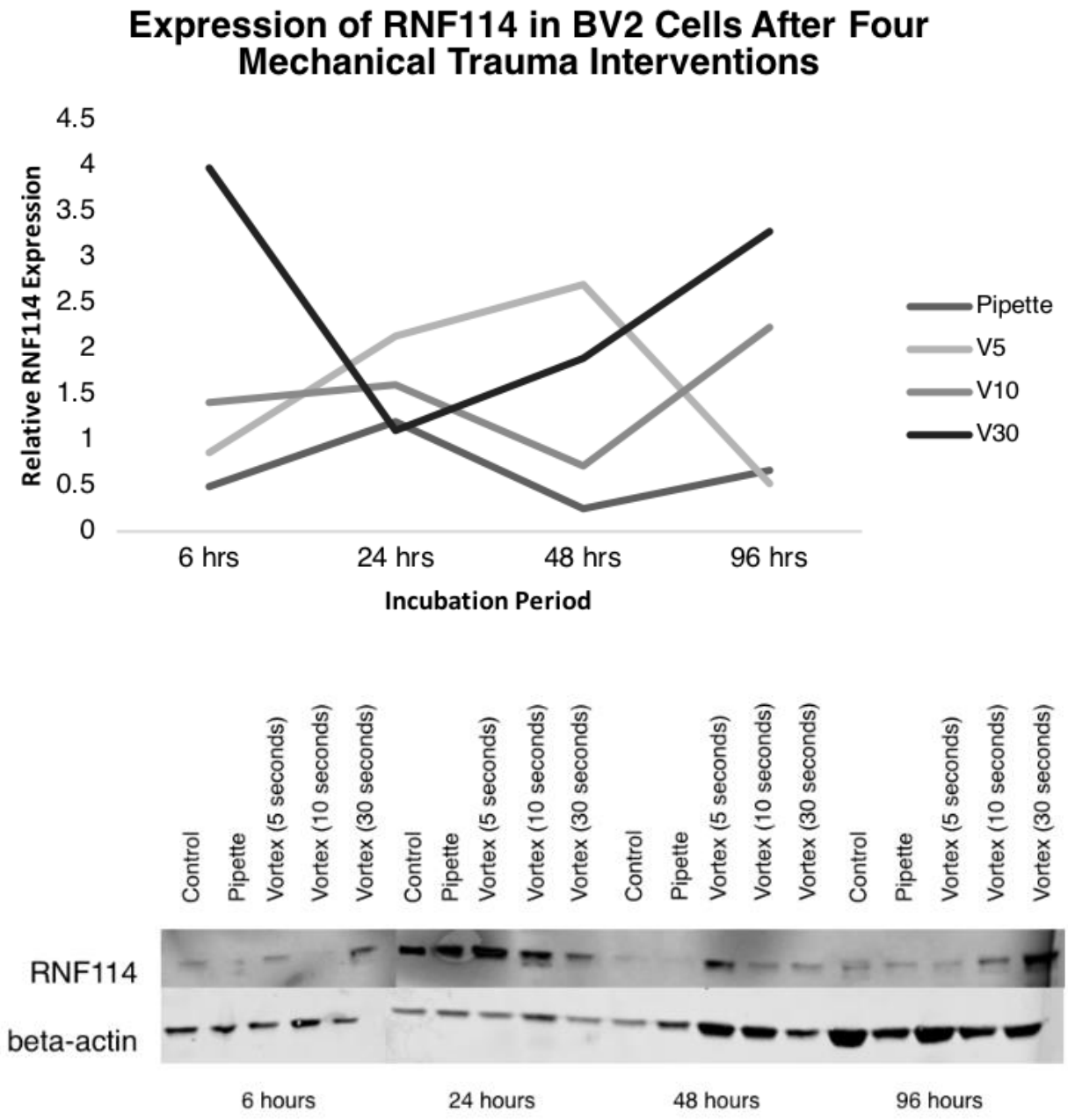


**Figure 9. Changes in expression of RNF114 after four mechanical trauma interventions**

BV2 cells were separated into six experimental conditions: control, vigorous resuspension with pipette (90 seconds), aeration of solution (90 seconds), and agitation of cells in a vortex machine (5 seconds, 10 seconds, and 30 seconds). Each experimental group was plated in 4 wells (2 x 12-well plate), then harvested and lysed at 6, 24, 48, and 96 hours post-intervention. Changes in expression of RNF114 were measured though western blotting (lower panel). Of these conditions, agitation of cells for thirty seconds using a vortex machine was found to correlate with an increase in RNF114 expression - 3.98x at 6 hours, 3.28x at 96 hours (upper panel).

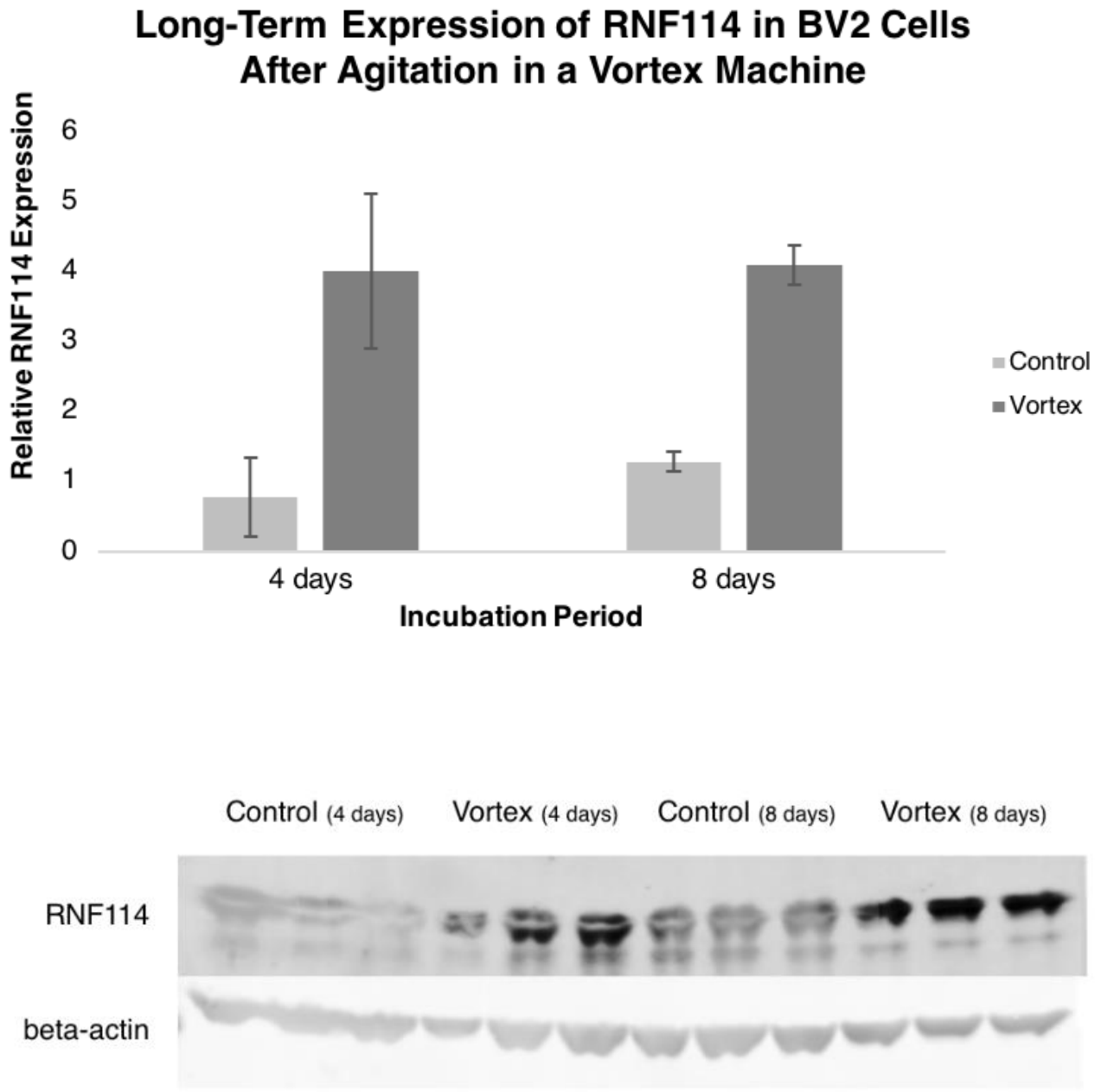


**Figure 10. Long-term changes in RNF114 expression after mechanical trauma intervention**

BV2 cells were separated into one of two experimental conditions: control and agitation of cells in a vortex machine (90 seconds). Cells were plated after the experiment, then harvested and passed to new plates at four and eight days post-intervention. Changes in expression of RNF114 were measured though western blotting (lower panel). A statistically significant increase in RNF114 expression was found at four (5.05x, p=0.0109) and eight (3.17x, p = 0.0008) days after initial intervention (upper panel).

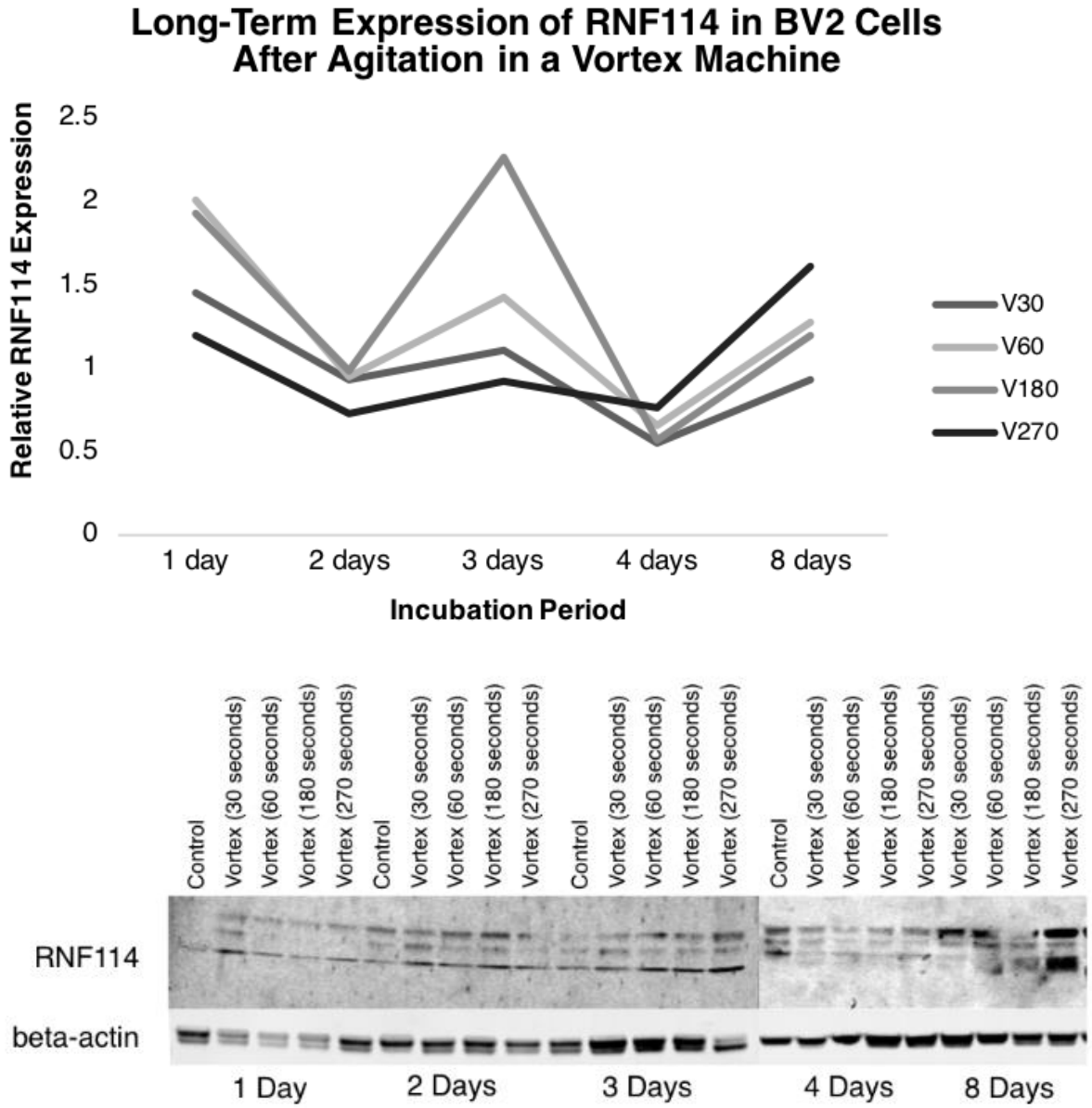


**Figure 11. Long-term effects of duration of agitation on RNF114 expression**

BV2 cells were separated into one of five experimental conditions: control and vortex (30, 60, 180, 270 seconds), then photographed and harvested at 1, 2, 3, 4, and 8 days after initial intervention. Changes in expression of RNF114 were measured though western blotting (lower panel). The difference between mean RNF114 expression in the control wells and RNF114 expression in each vortex condition (30, 60, 180, 270 seconds) averaged over time (1, 2, 3, 4, and 8 days) did not reach significance ($p = 0.9872, 0.2601, 0.2390, 0.3833$) (upper panel).

**Figure 12. Changes in BV2 cell morphology over an 8-day period after agitation in a vortex machine** (next page)

BV2 cells were separated into one of five experimental conditions: control and vortex (30, 60, 180, 270 seconds), then photographed and harvested at 1, 2, 3, 4, and 8 days after initial intervention. Examined under a Nikon Eclipse T51000 microscope, vortexed cells exhibited lower cell density than that of the control group, and the morphology of vortexed cells differed from that of the control cohort.

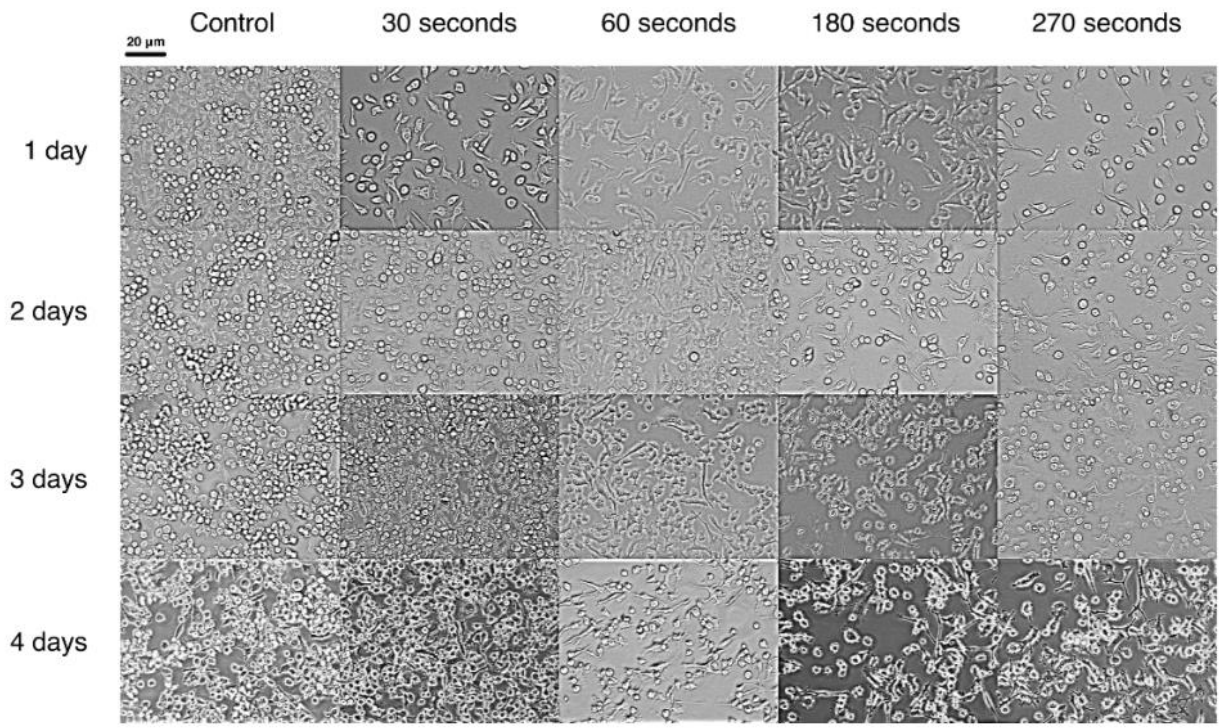
Control
30 seconds
60 seconds
180 seconds
270 seconds
20 µm
1 day
2 days
3 days
4 days

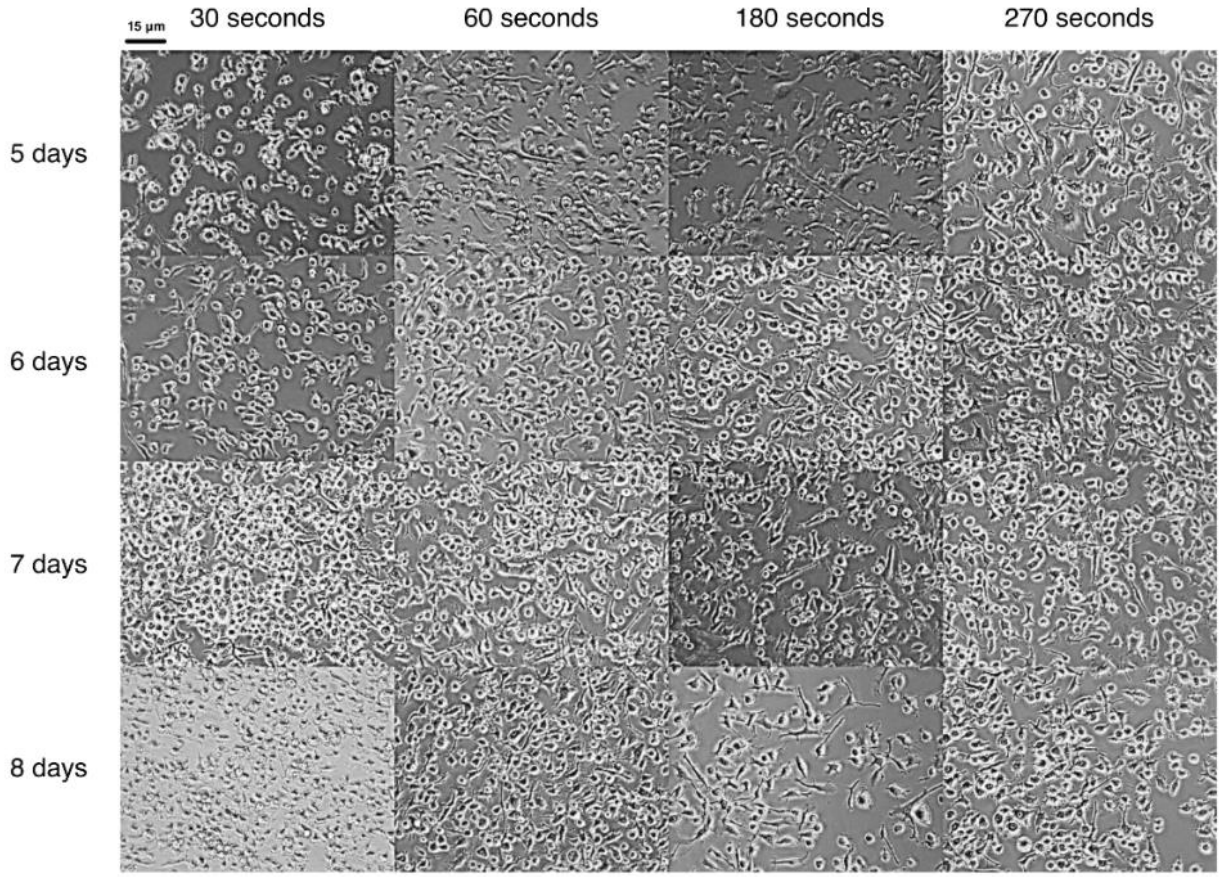
30 seconds
60 seconds
180 seconds
270 seconds
15 µm
5 days
6 days
7 days
8 days

## Discussion and Future Directions

### 1. Overview

In the present study, we set out to validate RNF114 expression data from the insoluble proteome, explore the relationship between RNF114 and NF-κB through transfection of plasmids and siRNA, measure the effect of RNF114 over-expression on aggregation of tau in a YFP/CFP HEK 293T tau biosensor line, and test a simple model of mechanical trauma in BV2 cell culture. When compared to control, expression of RNF114 in CTE homogenate was found to be significantly depressed, validating the initial finding from the insoluble proteome that expression of RNF114 is depressed in CTE. Transfection of RNF114 and NF-κB plasmids found that RNF114 inhibits the inflammatory response as a negative regulator of NF-κB. Additionally, transfection of a RNF114 plasmid in a tau biosensor line demonstrated that RNF114 up-regulation alone is not sufficient for aggregation of tau. Finally, we demonstrated a significant increase in expression of RNF114 after agitation of cells in a vortex machine at four and eight days after intervention, providing a foundation for future refinement and study of our mechanical trauma model.

### 2. Validation of Data from the CTE Insoluble Proteome

Taken together, the results of the four validation experiments support the finding that expression of RNF114 is depressed across all four stages of CTE in the insoluble proteome and establish a relationship between expression of RNF114 and expression of NF-κB. Initially, an IHC protocol was used to visualize expression of RNF114 in frontal cortex tissue sections from CTE and AD patients, but deposits of RNF114 were not visible in either group. This result could be attributed to a number of factors. First, the dilution of the RNF114 primary antibody used (1:500) and the duration of incubation (24 hours) could have been sub-optimal. Second, the RNF114 primary antibody could have been designed for western blotting and ICC but not for IHC staining.

Third, this result could be attributed to the down-regulation of RNF114 expression in CTE; in most conditions, labeling a down-regulated protein will be more difficult than labeling an over-expressed protein. In contrast to IHC staining of tissue sections, western blotting of brain homogenates and cell lysates allowed for precise measurement of RNF114 and NF-κB expression. When CTE homogenates were compared to control homogenates, expression of RNF114 in CTE was found to be significantly lower than in the control sample. As both the CTE and control groups drew from a wide variety of human patients and stages of disease, the results of this experiment support the finding that expression of RNF114 is depressed across all four stages of CTE in the insoluble proteome.

Comparisons of BV2 cell lysate and human brain homogenate established a relationship between expression of RNF114 and expression of NF-κB, but our experimental approach had some significant weaknesses. When BV2 cell lysate was compared to homogenate from the frontal cortex of one individual with CTE, RNF114 expression was found to be depressed in CTE, accompanied by a proportionate increase in expression of NF-κB. However, a number of factors limit the generalizability of these findings. First, BV2 cells are not equivalent to the wide variety of brain cells found in frontal cortex homogenate. Second, while the genomes of humans and mice share significant homology, unexpected differences in protein expression between these species represent a significant confounding variable. Third, only one source of CTE homogenate was used (8965) in these experiments, limiting the relevance of these findings to other CTE cases. Future studies that explore the relationship between RNF114 and NF-κB could draw from a more diverse sample of human CTE and control homogenates, addressing the weaknesses of the comparison conducted in this study.

**3. Transfection of Plasmid Over-Expression Constructs**

As a whole, the results of the plasmid over-expression experiments provide support for our first hypothesis, in which we proposed that up-regulation of RNF114 would directly affect expression of NF-κB. When BV2 cells were transfected with plasmids specific to RNF114, expression of RNF114 increased and expression of NF-κB decreased, suggesting that RNF114 serves as a negative regulator of NF-κB. When BV2 cells were transfected with plasmids specific of NF-κB, up-regulation of NF-κB elicited a proportionate increase in expression of RNF114, further supporting RNF114's proposed role as a negative regulator. While these results suggest a relationship between expression of RNF114 and expression of NF-κB, changes in protein expression after plasmid transfection in BV2 cells are not equivalent to the neuropathological changes that occur in humans and in animal models after rmTBI. Plasmid over-expression experiments capture short-term changes in protein expression (within two days of transfection), while repetitive trauma in animal models can be used to measure long-term changes in protein expression. In addition, the robust response of RNF114 to increased expression of NF-κB suggests that BV2 cells differ significantly from the brain cells of an individual with CTE; whereas RNF114 expression is depressed in CTE, leading to chronic inflammation, RNF114 is up-regulated in response to inflammatory stimuli in BV2 cells and is able to suppress the inflammatory response. Future studies could induce long-term up-regulation of RNF114 through repeated transfection of plasmids or lentiviral vectors specific to RNF114 and measure expression of NF-κB under these conditions. These experiments would better model the long-term effects of chronic inflammation on protein expression in BV2 cells.

ICC labeling allowed for visualization of protein expression in transfected BV2 cells. After transfection with the RNF114 plasmid, diffuse perinuclear and cytoplasmic deposits of RNF114

were observed in cells, and after transfection with the NF-κB plasmid, dense perinuclear and cytoplasmic deposits of NF-κB were observed in cells, accompanied by diffuse deposits of RNF114. While this result appears to confirm the success of the transfection protocol, an oversight in experimental design complicates this conclusion. All of the labeled cells had been transfected with either the RNF114 plasmid or the NF-κB plasmid before ICC staining, making comparison with a control group impossible; labeling RNF114 and NF-κB in a control group would provide additional insight into the efficacy of the transfection protocol.

Transfection of a HEK 293T tau biosensor line with an RNF114 plasmid and AD homogenate yielded mixed results. While there was not a statistically significant difference in tau aggregation between the control and plasmid conditions, there was a statistically significant difference in tau aggregation between the control and plasmid/homogenate conditions. These results fail to support our second hypothesis, in which we proposed that up-regulation of RNF114 alone would promote a significant increase in tau aggregation. However, the increase in tau aggregation after transfection with the plasmid and AD homogenate supports the template hypothesis of tau aggregation. While the significant increase in tau aggregation after transfection of the plasmid/homogenate mixture suggests that transfection was successful, transfection efficiency for the AD homogenate could have been higher than that of the RNF114 plasmid. Future studies could measure tau aggregation after plasmid transfection in other tau biosensor lines. As HEK 293T cells are derived from embryonic kidney cells, use of a neuronal tau biosensor line may yield results that are more relevant to the study of neurodegenerative diseases.

**4. Transfection of siRNA Duplexes**

Of the experiments conducted in the present study, RNAi knockdown of RNF114 expression was the most challenging, but the insights gained from these experiments provided a

clear foundation for further studies. In the first RNAi trial, the transfection of four siRNA duplexes in BV2 cells did not cause a statistically significant depression in expression of RNF114. Three possible factors leading to the failure of this experiment were proposed and tested. First, as siRNA duplexes could have degraded in the time between initial resuspension and transfection, concentration of each siRNA mixture was measured using a NanoDrop, and this possibility was ruled out. Second, as BV2 cells have a lower propensity for transfection than do HEK 293T cells, BV2 cells were replaced with HEK 293T cells in subsequent experiments to improve transfection efficiency. Third, as the initial incubation period of two days may not have been long enough for changes in protein expression to be reflected in a western blot, the incubation period was increased to three days in subsequent experiments.

The second RNAi trial was similarly unsuccessful; the transfection of four siRNA duplexes in HEK 293T cells did not cause a statistically significant depression in expression of RNF114. However, GFP, a marker of transfection efficiency, was highly expressed, suggesting that the transfection protocol was successful. The failure of the second experiment to produce a positive result narrowed the list of possible confounds to two main factors: either the siRNA duplexes were inactive, or the clearance of expressed RNF114 protein was low, leading residual RNF114 protein to appear on the western blot. While there is not a way to determine whether siRNA duplexes are active aside from transfection in cell culture, qPCR is able to measure knockdown of mRNA in real time, obviating the need for western blotting, and so was used in the next experiment.

As qPCR can measure knockdown of mRNA in real time, we relied on this method to quantify depression of RNF114 after siRNA transfection. After incubation, RNA was extracted from cells, converted to cDNA, and a qPCR protocol was conducted. Compared to a blank control, siRNA duplexes #1 and #3 caused a significant depression of mRNA synthesis, while the scramble

duplex (negative control) and siRNA duplex #2 did not. These results suggest that the siRNA duplexes #1 and #3 were active in previous experiments, but the knockdown of mRNA expression was not reflected in expression of RNF114 within the three-day incubation period. The failure of siRNA duplex #2 to knockdown mRNA expression can be attributed to a few possible factors. It is possible that siRNA duplex #2 was inactive. If the duplex was active, it is possible that the target cells failed to take up the duplex, or the duplex failed to engage with target mRNA. Using qPCR to verify mRNA knockdown, future studies could model the chronic depression of RNF114 expression observed in the insoluble proteome of CTE through the repeated transfection of target cells with siRNA. After a few weeks, repeated knockdown of mRNA through siRNA transfection would be reflected in expression of RNF114, and the effects of RNF114 knockdown on NF-κB expression and the inflammatory cascade could be explored.

**5. Modeling Mechanical Trauma in BV2 Cell Culture**

Attempts to model mechanical trauma in BV2 cell culture yielded promising, but mixed, results. BV2 cells were first separated into six experimental conditions: control, vigorous resuspension with pipette, aeration of solution, and agitation of cells in a vortex machine (for 5 seconds, 10 seconds, or 30 seconds) and harvested at 6, 24, 48, and 96 hours after the initial intervention. Of these conditions, agitation of cells for thirty seconds using a vortex machine correlated with an increase in RNF114 expression after intervention. While these results suggested a relationship between agitation with a vortex machine and up-regulation of RNF114 expression, there was only one sample for each condition and time point. In addition, this experiment only measured short-term cellular response (within 96 hours of the intervention). However, these results provided two important insights - first, other methods tested in this experiment (vigorous resuspension with pipette, aeration of solution) were unlikely to produce any meaningful

difference in expression of RNF114 in a larger study, and second, the response of BV2 cells to agitation in a vortex machine was dependent on the duration of agitation. These issues and insights were factored into the design of the next experiment.

Based on the results of the previous experiment, BV2 cells were then separated into two experimental conditions: control and agitation of cells in a vortex machine for 90 seconds. A statistically significant increase in RNF114 expression was found at both four and eight days after initial intervention. In addition, the decrease in expression of RNF114 between 4 and 8 days suggested that the cells began to recover from the initial trauma over time. This experiment provided clear support for our third hypothesis, in which we proposed that mechanical agitation of BV2 cell culture would lead to up-regulation of the inflammatory cascade and alter long-term expression of RNF114. Building on the success of the previous experiment, BV2 cells were separated into one of five experimental conditions - control and vortex for 30, 60, 180, or 270 seconds - then harvested at 1, 2, 3, 4, and 8 days after the initial intervention. While increased duration of agitation appeared to increase expression of RNF114, the difference between RNF114 expression in the control group and RNF114 expression in each vortex condition averaged over time was not statistically significant. As up-regulation of RNF114 expression varied across time points and experimental durations, these results suggested that there was not a linear relationship between duration of agitation and up-regulation of RNF114 expression, as previously assumed. Further studies are needed to explore this relationship.

While these experiments were limited by time constraints, future studies could evaluate this mechanical trauma model over a longer period of time, examine the effect of this model on different types of cell culture, and measure the effect of multiple interventions on the expression of RNF114 and NF-κB in BV2 cell culture. Experiments that measure expression of RNF114 and

NF-κB weeks after initial agitation of cell culture could provide key insights into the effect of mechanical trauma on long-term up-regulation of the inflammatory cascade. Additionally, experiments that involve repeated agitation of BV2 cells may better model the neurophysiological correlates of rmTBI. The agitation of BV2 cells described in this study provokes an acute response; to model repetitive trauma, target cells could be agitated multiple times over a period of weeks, and the expression of RNF114 and NF-κB could be measured at the end of the experimental period. Further studies are needed to explore this mechanical trauma model, and the three experiments described in this study provided a foundation for future research.

**Conclusion**

In the present study, we made three contributions to the CTE literature. First, we reviewed current rmTBI and CTE research, focusing on the history of CTE, the neurophysiological correlates of rmTBI, and the pathology and symptomology of CTE. Second, we examined the role of RNF114 and NF-κB in the inflammatory cascade and their possible link to CTE disease pathogenesis. In these experiments, we found that RNF114 inhibits the inflammatory response and serves as a negative regulator of NF-κB. Additionally, we measured the effect of RNF114 up-regulation on tau aggregation in a YFP/CFP HEK 293T tau biosensor line and found that up-regulation of RNF114 did not promote increased tau aggregation compared to control. Third, we developed a simple model for the mechanical induction of chronic inflammation in BV2 cell culture and demonstrated that agitation in a vortex machine led to elevated expression of RNF114 at four and eight days after intervention. Taken together, these findings suggest that RNF114 and NF-κB could play a role in the neuroinflammatory cascade and CTE pathogenesis, and the results of the mechanical trauma experiments provide a foundation for future development of cellular models of rmTBI.

**Works Cited**

Amadoro, Giuseppina, et al. "NMDA receptor mediates tau-induced neurotoxicity by calpain and ERK/MAPK activation." *Proceedings of the National Academy of Sciences of the United States of America* 103.8 (2006): 2892-2897.

Barkhoudarian, Garni, David A. Hovda, and Christopher C. Giza. "The molecular pathophysiology of concussive brain injury–an update." *Physical Medicine and Rehabilitation Clinics* 27.2 (2016): 373-393.

Baugh, Christine M., et al. "Current understanding of chronic traumatic encephalopathy." *Current treatment options in neurology* 16.9 (2014): 306.

Bijlmakers, Marie-José, et al. "Functional analysis of the RNF114 psoriasis susceptibility gene implicates innate immune responses to double-stranded RNA in disease pathogenesis." *Human molecular genetics* 20.16 (2011): 3129-3137.

Briggs, Denise I., Mariana Angoa-Pérez, and Donald M. Kuhn. "Prolonged Repetitive Head Trauma Induces a Singular Chronic Traumatic Encephalopathy–Like Pathology in White Matter Despite Transient Behavioral Abnormalities." *The American journal of pathology* 186.11 (2016): 2869-2886.

Blasi, E., et al. "An immortalized cell line expresses properties of activated microglial cells." *Journal of neuroscience research* 31.4 (1992): 616-621.

Byrnes, Kimberly R., et al. "Delayed mGluR5 activation limits neuroinflammation and neurodegeneration after traumatic brain injury." *Journal of neuroinflammation* 9.1 (2012): 43.

Cherry, Jonathan D., et al. "Microglial neuroinflammation contributes to tau accumulation in chronic traumatic encephalopathy." *Acta neuropathologica communications* (2016): 112.

Chen, Li-Jin, Yueh-Jan Wang, and Guo-Fang Tseng. "Compression alters kinase and phosphatase activity and tau and MAP2 phosphorylation transiently while inducing the fast adaptive dendritic remodeling of underlying cortical neurons." *Journal of neurotrauma* 27.9 (2010): 1657-1669.

Chen, L. P., P. S. Cai, and H. B. Liang. "Association of the genetic polymorphisms of NFKB1 with susceptibility to ovarian cancer." *Genet Mol Res* 14.3 (2015): 8273-8282.

Chen, Ying, et al. "The NFKB1 polymorphism (rs4648068) is associated with the cell proliferation and motility in gastric cancer." *BMC gastroenterology* 15.1 (2015): 21.

Coons, Albert H., et al. "The demonstration of pneumococcal antigen in tissues by the use of fluorescent antibody." *J. Immunol* 45.3 (1942): 159-170.

Corsellis, J. A. N., C. J. Bruton, and Dorothy Freeman-Browne. "The aftermath of boxing." *Psychological medicine* 3.3 (1973): 270-303.

Courville, C. B. "Punch drunk. Its pathogenesis and pathology on the basis of a verified case." *Bulletin of the Los Angeles Neurological Society* 27 (1962): 160-168.

Critchley, M. "Punch-drunk syndromes: the chronic traumatic encephalopathy of boxers." *Hommage a Clovis Vincent* (1949): 131-141.

Daneshvar, Daniel, et al. "Alzheimer's disease, Lewy body disease and TDP43 proteinopathy following a single TBI." *Alzheimer's & Dementia: The Journal of the Alzheimer's Association* 9.4 (2013): P438.

Daneshvar, Daniel, et al. "Post-traumatic neurodegeneration and chronic traumatic encephalopathy." *Molecular and Cellular Neuroscience* 66 (2015): 81-90.

Dam, Sharmistha, et al. "The Influenza A Virus Genotype Determines the Antiviral Function of NF-κB." *Journal of virology* 90.17 (2016): 7980-7990.

Dohi, Kenji, et al. "Gp91 phox (NOX2) in classically activated microglia exacerbates traumatic brain injury." *Journal of neuroinflammation* 7.1 (2010): 41.

Faden, Alan I., et al. "The role of excitatory amino acids and NMDA receptors in traumatic brain injury." *Science* 244.4906 (1989): 798-800.114. Chronic traumatic encephalopathy in athletes -progressive tauopathy after repetitive head injury

Faden, Alan I., and David J. Loane. "Chronic neurodegeneration after traumatic brain injury: Alzheimer disease, chronic traumatic encephalopathy, or persistent neuroinflammation?." *Neurotherapeutics* 12.1 (2015): 143-150.

Gaetz, Michael. "The multi-factorial origins of Chronic Traumatic Encephalopathy (CTE) symptomology in post-career athletes: The athlete post-career adjustment (AP-CA) model." *Medical hypotheses* 102 (2017): 130-143.

Gilmore, Thomas D. "Introduction to NF-κB: players, pathways, perspectives." *Oncogene* 25.51 (2006): 6680.

Goldstein, Lee E., et al. "Chronic traumatic encephalopathy in blast-exposed military veterans and a blast neurotrauma mouse model." *Science translational medicine* 4.134 (2012): 134ra60-134ra60.

Graham, Frank L., and Alex J. van der Eb. "A new technique for the assay of infectivity of human adenovirus 5 DNA." *Virology* 52.2 (1973): 456-467.

Hales, Chadwick, et al. "Late-stage CTE pathology in a retired soccer player with dementia." *Neurology* 83.24 (2014): 2307-2309.

Hales, Chadwick, et al. "Characterization of Detergent Insoluble Proteome in Chronic Traumatic Encephalopathy." *Journal of Neuropathology & Experimental Neurology* 77.1 (2017): 40-49.

Han, J., et al. "ZNF313 is a novel cell cycle activator with an E3 ligase activity inhibiting cellular senescence by destabilizing p21 WAF1." *Cell death and differentiation* 20.8 (2013): 1055.

Harhaj, Edward W., and Vishva M. Dixit. "Regulation of NF-κB by deubiquitinases." *Immunological reviews* 246.1 (2012): 107-124.

Held, Paul. "An introduction to fluorescence resonance energy transfer (FRET) technology and its application in bioscience." *Bio-Tek Application Note* (2005).

Henn, Anja, et al. "The suitability of BV2 cells as alternative model system for primary microglia cultures or for animal experiments examining brain inflammation." *ALTEX: Alternatives to animal experimentation* 26.2 (2009): 83-94.

Holmes, Brandon B., et al. "Proteopathic tau seeding predicts tauopathy in vivo." *Proceedings of the National Academy of Sciences* 111.41 (2014): E4376-E4385.

Housley, William J., et al. "Genetic variants associated with autoimmunity drive NFκB signaling and responses to inflammatory stimuli." *Science translational medicine* 7.291 (2015): 291ra93-291ra93.

Huber, Bertrand R., et al. "Potential long-term consequences of concussive and subconcussive injury." *Physical Medicine and Rehabilitation Clinics* 27.2 (2016): 503-511.

Hussain, Syed Arshad. "An introduction to fluorescence resonance energy transfer (FRET)." *arXiv preprint arXiv:0908.1815* (2009).

Hutchison, Michael G., et al. "Systematic review of mental health measures associated with concussive and subconcussive head trauma in former athletes." *International journal of psychophysiology* (2017).

Iliff, Jeffrey J., et al. "Impairment of glymphatic pathway function promotes tau pathology after traumatic brain injury." *Journal of Neuroscience* 34.49 (2014): 16180-16193.

Johnson, Victoria E., et al. "Inflammation and white matter degeneration persist for years after a single traumatic brain injury." *Brain* 136.1 (2013): 28-42.

Kanaan, Nicholas M., et al. "Pathogenic forms of tau inhibit kinesin-dependent axonal transport through a mechanism involving activation of axonal phosphotransferases." *Journal of Neuroscience* 31.27 (2011): 9858-9868.

Kanzaki, Hirotaka, et al. "Trastuzumab-Resistant Luminal B Breast Cancer Cells Show Basal-Like Cell Growth Features Through NF-κB-Activation." *Monoclonal antibodies in immunodiagnosis and immunotherapy* 35.1 (2016): 1-11.

Kfoury, Najla, et al. "Trans-cellular propagation of Tau aggregation by fibrillar species." *Journal of Biological Chemistry* 287.23 (2012): 19440-19451.

Lamond, Angus. "FRET Measurement between YFP and CFP." *Lamond Lab*, www.lamondlab.com/newwebsite/ProtocolsforWebsite/FRETmeasurementbetweenYFPandCFP.pdf.

Li, Peng, and Zhaohui Li. "Effects of NF-κB and hypoxia on the biological behavior of Y79 retinoblastoma cells." *International journal of clinical and experimental pathology* 8.2 (2015): 1725.

Li, Ping, Ying Wang, and Justin H. Turner. "Proinflammatory mediators alter expression of nuclear factor kappa B–regulating deubiquitinases in sinonasal epithelial cells." *International forum of allergy & rhinology*. Vol. 5. No. 7. 2015.

Loane, David J., et al. "Progressive neurodegeneration after experimental brain trauma: association with chronic microglial activation." *Journal of Neuropathology & Experimental Neurology* 73.1 (2014): 14-29.

Mahar, Ian, Michael L. Alosco, and Ann C. McKee. "Psychiatric phenotypes in chronic traumatic encephalopathy." *Neuroscience & Biobehavioral Reviews* (2017).

Mahmood, Tahrin, and Ping-Chang Yang. "Western blot: technique, theory, and trouble shooting." *North American journal of medical sciences* 4.9 (2012): 429.

Manavalan, Arulmani, et al. "Brain site-specific proteome changes in aging-related dementia." *Experimental & molecular medicine* 45.9 (2013): e39.

Martínez-Pérez, R., et al. "Chronic traumatic encephalopathy: The unknown disease." *Neurología (English Edition)* 32.3 (2017): 185-191.

Martland, Harrison S. "Punch drunk." *Journal of the American Medical Association* 91.15 (1928): 1103-1107.

McKee, Ann C., et al. "Chronic traumatic encephalopathy in athletes: progressive tauopathy after repetitive head injury." *Journal of Neuropathology & Experimental Neurology* 68.7 (2009): 709-735.

McKee, Ann C., et al. "Clinicopathological evaluation of chronic traumatic encephalopathy in players of American football." *Jama* 318.4 (2017): 360-370.

McKee, Ann C., et al. "TDP-43 proteinopathy and motor neuron disease in chronic traumatic encephalopathy." *Journal of Neuropathology & Experimental Neurology* 69.9 (2010): 918-929.

McKee, Ann C., et al. "The first NINDS/NIBIB consensus meeting to define neuropathological criteria for the diagnosis of chronic traumatic encephalopathy." *Acta neuropathologica* 131.1 (2016): 75-86.

McKee, Ann C., et al. "The spectrum of disease in chronic traumatic encephalopathy." *Brain* 136.1 (2013): 43-64.

McKee, Ann C., and Daniel H. Daneshvar. "The neuropathology of traumatic brain injury." *Handbook of clinical neurology*. Vol. 127. Elsevier, 2015. 45-66.

Mez, Jesse, et al. "Assessing clinicopathological correlation in chronic traumatic encephalopathy: rationale and methods for the UNITE study." *Alzheimer's research & therapy* 7.1 (2015): 62.

Millspaugh, J. A. "Dementia pugilistica." *US Naval Med Bull* 35.297 (1937): e303.

Milstein, Stuart, et al. "Measuring RNAi knockdown using qPCR." *Methods in enzymology*. Vol. 533. Academic Press, 2013. 57-77.

Monroe, Margo R. "Plasmids 101: What Is a Plasmid?" *AddGene*, blog.addgene.org/plasmids-101-what-is-a-plasmid.

Mouzon, Benoit C., et al. "Chronic neuropathological and neurobehavioral changes in a repetitive mild traumatic brain injury model." *Annals of neurology* 75.2 (2014): 241-254.

Morganti-Kossmann, Maria Cristina, et al. "Inflammatory response in acute traumatic brain injury: a double-edged sword." *Current opinion in critical care* 8.2 (2002): 101-105.

Nettleship, Joanne E., et al. "Transient expression in HEK 293 cells: an alternative to E. coli for the production of secreted and intracellular mammalian proteins." Insoluble proteins. Humana Press, New York, NY, 2015. 209-222.

Nizynski, Bartosz, Wojciech Dzwolak, and Krzysztof Nieznanski. "Amyloidogenesis of Tau protein." *Protein Science* (2017).

Ojo, Joseph O., Benoit C. Mouzon, and Fiona Crawford. "Repetitive head trauma, chronic traumatic encephalopathy and tau: Challenges in translating from mice to men." *Experimental neurology* 275 (2016): 389-404.

Omalu, Bennet I., et al. "Chronic traumatic encephalopathy in a National Football League player." Neurosurgery 57.1 (2005): 128-134.

Osnato, M., and Gilberti, V. Postconcussion Neurosis–Traumatic Encephalitis. *Arch. Neurol, and Psych.*, 1927, xviii, 181.

"Overview of Immunohistochemistry (IHC)." *Thermo Fisher Scientific*.

"Overview of Western Blotting." *Thermo Fisher Scientific*.

Perkins, Neil D. "The Rel/NF-κB family: friend and foe." *Trends in biochemical sciences* 25.9 (2000): 434-440.

Perkins, N. D., and T. D. Gilmore. "Good cop, bad cop: the different faces of NF-κB." *Cell death and differentiation* 13.5 (2006): 759.

Piao, Chun-Shu, et al. "Late exercise reduces neuroinflammation and cognitive dysfunction after traumatic brain injury." *Neurobiology of disease* 54 (2013): 252-263.

Pullman, M. Y., et al. "Antemortem biomarker support for a diagnosis of clinically probable chronic traumatic encephalopathy." (2017): 638.

Ramlackhansingh, Anil F., et al. "Inflammation after trauma: microglial activation and traumatic brain injury." *Annals of neurology* 70.3 (2011): 374-383.

Renner, Florian, and M. Lienhard Schmitz. "Autoregulatory feedback loops terminating the NF-κB response." *Trends in biochemical sciences* 34.3 (2009): 128-135.

"RNA Interference (RNAi)." *National Center for Biotechnology Information*, U.S. National Library of Medicine, www.ncbi.nlm.nih.gov/probe/docs/techrnai/.

Rodriguez, M. S., et al. "The RING ubiquitin E3 RNF114 interacts with A20 and modulates NF-κB activity and T-cell activation." *Cell death & disease* 5.8 (2014): e1399.

Rubenstein, Richard, et al. "Tau phosphorylation induced by severe closed head traumatic brain injury is linked to the cellular prion protein." *Acta neuropathologica* (2017): 30.

Sen, Ranjan, and David Baltimore. "Inducibility of κ immunoglobulin enhancer-binding protein NF-κB by a posttranslational mechanism." *Cell* 47.6 (1986): 921-928.

Seo, Jeong-Sun, et al. "Transcriptome analyses of chronic traumatic encephalopathy show alterations in protein phosphatase expression associated with tauopathy." *Experimental & molecular medicine* 49.5 (2017): e333.

Shaw, Gerry, et al. "Preferential transformation of human neuronal cells by human adenoviruses and the origin of HEK 293 cells." The FASEB Journal 16.8 (2002): 869-871.

Shembade, Noula, and Edward W. Harhaj. "Regulation of NF-κB signaling by the A20 deubiquitinase." *Cellular & molecular immunology* 9.2 (2012): 123.

Shimozono, Satoshi, and Atsushi Miyawaki. "Engineering FRET constructs using CFP and YFP." *Methods in cell biology* 85 (2008): 381-393.

Shitaka, Yoshitsugu, et al. "Repetitive closed-skull traumatic brain injury in mice causes persistent multifocal axonal injury and microglial reactivity." *Journal of Neuropathology & Experimental Neurology* 70.7 (2011): 551-567.

Stansley, Branden, Jan Post, and Kenneth Hensley. "A comparative review of cell culture systems for the study of microglial biology in Alzheimer's disease." *Journal of neuroinflammation* 9.1 (2012): 115.

Stein, Thor D., et al. "Beta-amyloid deposition in chronic traumatic encephalopathy." *Acta neuropathologica* 130.1 (2015): 21-34.

Stein, Thor D., Victor E. Alvarez, and Ann C. McKee. "Concussion in chronic traumatic encephalopathy." *Current pain and headache reports* 19.10 (2015): 47.

Stern, Robert A., et al. "Clinical presentation of chronic traumatic encephalopathy." *Neurology* 81.13 (2013): 1122-1129.

Stern, Robert A., et al. "Long-term consequences of repetitive brain trauma: chronic traumatic encephalopathy." *Pm&r* 3.10 (2011): S460-S467.

Stuart, Philip E., et al. "Genome-wide association analysis identifies three psoriasis susceptibility loci." *Nature genetics* 42.11 (2010): 1000.

Tadross, Michael R., et al. "Robust approaches to quantitative ratiometric FRET imaging of CFP/YFP fluorophores under confocal microscopy." *Journal of microscopy* 233.1 (2009): 192-204

Taylor, Sean C., and Anton Posch. "The design of a quantitative western blot experiment." BioMed research international 2014 (2014).

"Transfection Methods." *Thermo Fisher Scientific*.

Vereecke, Lars, Rudi Beyaert, and Geert van Loo. "Genetic relationships between A20/TNFAIP3, chronic inflammation and autoimmune disease." (2011): 1086-1091.

Vereecke, Lars, Rudi Beyaert, and Geert van Loo. "The ubiquitin-editing enzyme A20 (TNFAIP3) is a central regulator of immunopathology." *Trends in immunology* 30.8 (2009): 383-391.

Verstrepen, Lynn, et al. "Expression, biological activities and mechanisms of action of A20 (TNFAIP3)." *Biochemical pharmacology* 80.12 (2010): 2009-2020.

Willis, M. D., and N. P. Robertson. "Chronic traumatic encephalopathy: identifying those at risk and understanding pathogenesis." *Journal of neurology* 264.6 (2017): 1298-1300.

Wilson, Lindsay, et al. "The chronic and evolving neurological consequences of traumatic brain injury." *The Lancet Neurology* 16.10 (2017): 813-825.

Wojnarowicz, Mark W., et al. "Considerations for Experimental Animal Models of Concussion, Traumatic Brain Injury, and Chronic Traumatic Encephalopathy—These Matters Matter." *Frontiers in neurology* 8 (2017): 240.

Woodcock, Thomas, and Cristina Morganti-Kossmann. "The role of markers of inflammation in traumatic brain injury." *Frontiers in neurology* 4 (2013): 18.

Xu, Zhiming, et al. "Sesamin protects SH-SY5Y cells against mechanical stretch injury and promoting cell survival." *BMC neuroscience* 18.1 (2017): 57.

Zaynagetdinov, Rinat, et al. "Chronic NF-κB activation links COPD and lung cancer through generation of an immunosuppressive microenvironment in the lungs." *Oncotarget* 7.5 (2016): 5470.

Zhang, Run, et al. "Anti-inflammatory and immunomodulatory mechanisms of mesenchymal stem cell transplantation in experimental traumatic brain injury." *Journal of neuroinflammation* 10.1 (2013): 871.

Zhang, Ye, et al. "An RNA-sequencing transcriptome and splicing database of glia, neurons, and vascular cells of the cerebral cortex." *Journal of Neuroscience* 34.36 (2014): 11929-11947.

Ziebell, Jenna M., and Maria Cristina Morganti-Kossmann. "Involvement of pro-and anti-inflammatory cytokines and chemokines in the pathophysiology of traumatic brain injury." *Neurotherapeutics* 7.1 (2010): 22-30.